2011

Modeling effects of coupled convection and CO2 injection in stimulating geopressured geothermal reservoirs

Tatyana Plaksina
Louisiana State University and Agricultural and Mechanical College

MODELING EFFECTS OF COUPLED CONVECTION AND CO_2 INJECTION IN STIMULATING GEOPRESSURED GEOTHERMAL RESERVOIRS

A Thesis

Submitted to the Graduate Faculty of the
Louisiana State University and
Agricultural and Mechanical College
in partial fulfillment of the
requirements for the degree of

Master of Science in Petroleum Engineering

in

The Craft & Hawkins Department of Petroleum Engineering

by
Tatyana Plaksina
B.A., Mathematics and Computer Science, Lawrence University, Appleton, WI, 2005
August 2011

Acknowledgements

I would like to express my gratitude to my committee members, Drs. Christopher White, Mayank Tyagi, Mileva Radonjic, and Jeffrey Hanor, for their guidance. In particular, I thank my advisor and committee chair Dr. White for providing excellent advice and facilitating my professional growth throughout my stay at LSU. I also would like to acknowledge Dr. Tyagi for his help in multiple aspects of numerical simulation and inspiration. It is my pleasure to thank Dr. Radonjic for her emotional support and valuable academic advice. My special acknowledgement goes to Dr. Hanor for his patience, research insight and input.

The author is also grateful for Chevron Endowed Professorship for providing financial support. It sponsored my travel and participation in TOUGH2 workshop conducted in Berkeley National Laboratory, Berkeley, CA in September 2009. Funds of this professorship also gave me an opportunity to present an extract of this thesis at Stanford Geothermal Workshop in Palo Alto, CA in February 2011. Without this valuable support from Chevron this research would not be possible.

Finally, I would like to thank my family members for their help, love, and support in all my endeavors.

Contents

List of Tables

List of Figures

Abstract

Geopressured geothermal brines are a vast geothermal resource in the US Gulf of Mexico region. In particular, geopressured sandstones near salt domes are potential sources of geothermal energy because salt diapirs with high thermal conductivities may pierce younger, cooler strata. These characteristics enhance transfer heat from older, hotter strata at the base of the diapir into shallower strata. Moreover, widespread geopressure in the Gulf region tends to preserve permeability, enhancing productivity. As an example, the Camerina A sand of South Louisiana was chosen as a geomodel for a numerical simulation study of effects of CO_2 injection and coupled convection as a method of geothermal development. This study presents scenarios for heat harvesting from typical Gulf of Mexico aquifers including Camerina A that take advantage of coupled convection and simultaneous CO_2 sequestration. Suites of TOUGH2 numerical simulations demonstrate benefits of introducing CO_2 injection wells, varying locations of injection/production wells, and exploiting gravity segregation of the fluids.

Chapter 1

Introduction

1.1 Motivation and Objective

Geothermal systems provide abundant and carbon-free thermal energy for electricity generation, space heating and air-conditioning. According to the most recent and conservative USGS estimate, in the US alone the geothermal resource base of the crust down to 10 km comprises about 13.5 million exajoules[1] or quads (MIT 2006). This amount of energy is equivalent to that stored in 2.5×10^{15} barrels of oil, 4.86×10^{14} tons of coal, or 1.35×10^{16} Mscf of natural gas. Despite these impressive figures, geothermal energy harvesting is mostly confined to a few high-grade (high-enthalpy or high temperature) hydrothermal and hot dry rock fields, leaving other geothermal systems virtually untapped.

One underexploited type of geothermal systems is geopressured sedimentary aquifers. Geopressured aquifers are undercompacted, brine-saturated, porous, and permeable formations that have anomalously high pore pressures and temperatures over 100°C. Geofluids in these systems tend to have high salinities and concentrations of dissolved gases. Geopressured fields are considered a medium- and low-grade (or low-enthalpy) geothermal resource. They occupy vast subsurface areas in coastal regions, and in the US contain approximately 170,000 EJ of energy. The US states of Louisiana and Texas are examples of geographic locations where geopressured systems occur frequently.

Several major technical obstacles render many low-grade geopressured systems subcommercial. These include a necessity to drill multiple wells to access remote parts of a reservoir in order to improve heat sweep, the high cost of pressure maintenance programs, and burdensome surface handling of withdrawn geofluids. Low-enthalpy systems have lower heat content and thermal efficiency. In addition to these problems, geothermal development might cause land subsidence due to compaction in the producing geologic formation. As a result, pilot commercial projects exploit only those sites that have anomalously high geothermal gradients and strong water drives the so-called "low-hanging fruit" of the tremendous resource. This study investigates a new method to improve heat recovery from the geopressured aquifers by combining the effects of natural and forced convection. More specifically, it demonstrates advantages of characterizing a natural convection pattern within the formation of interest and using the obtained results for subsequent heat extraction by means of coupled convection. This approach allows for a better geothermal resource estimation and selection of a

[1] 1 exajoule = 10^{18} joules

more efficient production arrangement.

Because the current study might be particularly beneficial for development of the local energy potential, the geomodels investigated here have petrophysical and thermodynamic properties of geopressured formations found in the Gulf of Mexico region. Though mostly focused on the coupled convection production technique, this study also discusses supplementary methods for development of hot saline aquifers including CO_2 sequestration simultaneous with heat harvesting. It provides a discussion and analysis of the effect of the formation dip on heat recovery as well. One South Louisiana saline aquifer, the Camerina A, is a central example for this study, and is used for a more detailed investigation of an optimal geothermal production scenario.

Although this piece of research is not related directly to oil and gas development, there is a reason why a petroleum engineer should undertake it. Similarly to petroleum reservoir engineering, in geothermal reservoir engineering the primary task is to access a natural resource through the wellbore. In the first case the resource is hydrocarbon, in the latter - hot geofluid. The parallel between the two types of problems can be extended further, because both of them require estimation of the resource size, building geomodels, running numerical simulations with subsequent sensitivities study, and, finally, proposing an optimal resource development scenario. Thus, expertise accumulated in petroleum reservoir engineering discipline can be applied directly to the problems in geothermal engineering.

1.2 Thesis Outline

The structure of this thesis leads the reader from a general overview of fluid convection to an in-depth analysis of this phenomenon in geopressured geothermal reservoirs. Chapter **2** provides a succinct summary of geopressured geothermal resource distribution and present day practices and challenges in its development. Following this short introduction, some key theoretical concepts are discussed. Those include qualitative and quantitative methods for describing natural and forced convection in flat and dipping porous media. This chapter also contains a survey of literature concerning compositionally-driven convection and, more specifically, energy transfer across the reservoir due to CO_2 injection. At the end of the chapter the reader is familiarized with software tools and experimental designs chosen for numerical modeling.

Chapter **3** elaborates further on the theoretical framework and presents the procedure for characterizing natural convection. A suite of 2D TOUGH2 simulations for systems with varying geometries and petrophysical properties reveal primary heat transport mechanisms, importance of boundary layers and duration of the idle period when the geothermal systems are quiescent. The last part of the chapter focuses on characterization of convection pattern for the local example Camerina A sand and examines feasibility of geothermal development based on wellbore cooling technique. After the detailed investigation of effects and modeling of natural convection, the emphasis shifts from quiescent reservoir simulation to production scenarios modeling. Chapter **4** describes the experimental design for geothermal production cases that take advantage of both natural and forced convection. Later in the chapter the possibility of simultaneous heat harvesting and CO_2 sequestration is investigated. The final part of the thesis comprises Chapters **5**, **6** and **7** that present sensitivity studies, qualitative analysis of the results, and further research recommendations.

Chapter 2

Convection in Porous Media

This chapter provides a summary of reports, articles and book chapters necessary to understand the context of the stated problem and the outlined objectives. First, the reader is introduced to a description of geopressured geothermal energy and some technical difficulties that inhibit wide commercialization of this low-enthalpy resource in the Gulf coast. Second, the discussion proceeds with an overview of research devoted to convection in flat and inclined porous media caused by thermal effects. Finally, several works on CO_2-driven convection in water and brine and the greenhouse gas sequestration are reviewed. The chapter ends with a brief description of the software TOUGH2 chosen for modeling and justification of this choice.

2.1 Geopressured Geothermal Resource

In response to recent fluctuations in hydrocarbon prices and growing interest of the society in environmentally-friendly energy sources, a number of researchers turned back to a study of geothermal systems which was mostly abandoned in the 1980s. Despite some discrepancies in research terminology, most publications agree on key definitions that are instrumental for the further discussion. A *geothermal system* is defined as a geologic assembly of subsurface components including a source or sources of geofluid, hydrologic flow paths, and possible discharge regions (Grant 1982). The term *geothermal reservoir* describes a part of a geothermal system from which mass and/or heat can be produced.

For classification purposes, researchers divide geothermal systems into several different types according to their geologic features and fluid drive mechanisms. Among these types are *hydrothermal*, *hot dry rock*, and *geopressured* reservoirs. Since this study focuses exclusively on geopressured resource, the following overview will pertain to this type of geothermal systems only.

In geographic areas with deep sedimentary basins development of geothermal resource is usually separated into two main categories: coproduced fluids and geopressured geothermal extraction. Projects falling into the first category produce geothermal energy from hot water which is a by-product of oil and gas development. As a rule, this type of geothermal resource exploitation is confined to existing hydrocarbon fields at depths between 4 to 6 km (MIT 2006). Curtice and Dalrymple (2004) summarize that in the US only the annual volume of coproduced hot water reaches 33 billion barrels. They also convert this raw thermal energy into electric power and obtain an equivalent of about 3,000 MW per year (this calculation is based on geofluid with temperature of 100℃). Geothermal projects that belong to the second category are independent of oil and gas production and exploit thermal potential of saline aquifers. Geopressured hot saline aquifers are common in deep sedimentary basins such as the Northern Gulf of Mexico basin with formation pressures above hydrostatic and temperatures above 100℃. The Northern Gulf of Mexico basin is a vast geopressured subsurface region that occupies more than 145,000 km^2 and, according to conservative estimate of White and Williams (1975), stores raw thermal energy of about 46,000 EJ or electric power equivalent of 10 MW per year.

These types of geothermal reservoirs seem to be very similar for production purposes and this study can be applied to both of them. The main consideration to keep in mind, however, is when the proposed initialization method is relevant. One of the objectives of this research is to demonstrate importance of initializing geomodels with proper temperatures distribution achieved by idling the systems for a substantial time period (from 100 to millions of years). Because the thermal profile of the first category of geothermal reservoirs is distorted by oil and gas production, initialization with the idle period does not provide a realistic temperature distribution. Thus, application of the initialization assumes that geothermal systems did not experience forced convection (due to injection or withdrawal of geofluid) prior to heat harvesting.

2.1.1 Local Development Opportunity - the Camerina A Sand

The introductory chapter states that one of the objectives of this study is to attract attention to the local geothermal potential. In connection to this objective, it is natural to provide an example of a hot saline aquifer in the Gulf coast of Louisiana suitable for heat extraction with the proposed method. Based on recent geothermal research at LSU Department of Geology and Geophysics, the Camerina A sand of South Louisiana is selected as a base case.

The Camerina A sand is a Late Oligocene deposit identified near Gyuedan salt dome in Vermillion parish, LA (Fig. 2.1) at an approximate true vertical depth of 4300 m (Gray 2010). Its depositional environment can be described as a delta front to distributary mouth bar and it is a part of a marine transgressive sequence. The sand's average thickness is about 100 m, permeability is 200 mD and its porosity varies between 9 to 31 percent. The Camerina A sand is a dipping aquifer with varying dips ranging between 1.2 to 28 degrees. The corrected formation temperature is close to 140 ℃ with a geothermal gradient of about 29 ℃/km and estimated formation pressure is over 80 MPa (Gray 2010).

Despite the fact that the Camerina A sand is located in a geographic area where relatively low geothermal gradients are expected, the temperature of the aquifer's fluid is suitable for geothermal development via an organic binary cycle electricity generation plant (MIT 2006). This anomaly might be a result of the sand's proximity to the salt domes that cause elevated temperatures in sediments adjacent to their flanks. Research on salt domes and thermal anomalies created by them suggests that salt's high thermal conductivity might cause temperature differences up to 30 ℃ in comparison to surrounding deposits and transfer heat to adjacent aquifers (Gray 2010). the Camerina A sand combines all the properties pertaining to the objectives of this study (dip, anomalously high formation temperature suitable for electricity generation, substantial thickness and areal extent) and, therefore, its geomodel is used in the analysis of an optimal heat harvesting scenario with zero net mass

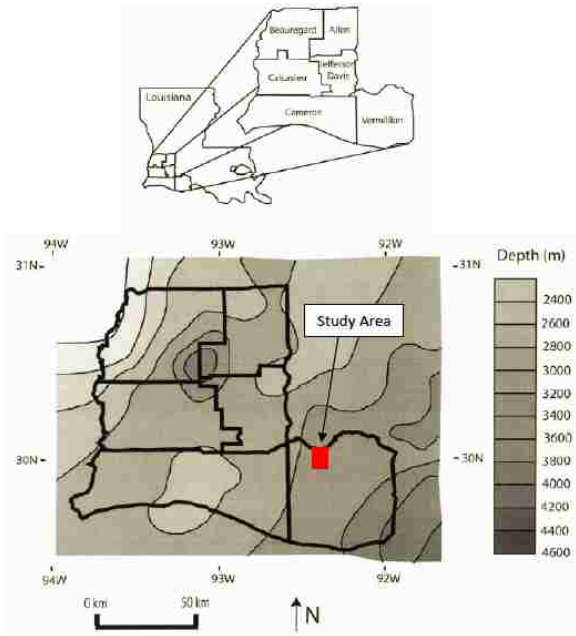

Figure 2.1: 100°C isotherm map of the study area. Modified from Szalkowski and Hanor (2003)

withdrawal.

2.2 Natural Convection in Flat and Inclined Systems

Because the proposed geothermal production method relies on zero net mass withdrawal from the formation of interest and strategic placement of wells for improved heat sweep, it is important to consider natural fluid convection as a thermal energy drive mechanism. Natural convection is sometimes also called thermally-driven convection. This physical phenomenon results from non uniform heating of a porous medium saturated with a fluid, density of which is temperature dependent. In connection to convective effects in geothermal systems, it is appropriate to mention Horne's work (Horne 1975), a primary focus of which is two- and three-dimensional modeling of transient behavior in convection-dominated natural systems.

Horne's findings are better understood in the context of governing equations of fluid flow through porous media. Grant (1982) provides a succinct summary of geothermal reservoir dynamics and outlines major equations of motion and state. Conservation of mass for single- and two-phase flows are

$$\phi \frac{\partial \rho}{\partial t} + \nabla \cdot u = 0 \tag{2.1}$$

and

$$\phi \frac{\partial}{\partial t}(\rho_w S_w + \rho_s S_s) + \nabla \cdot (u_s + u_w) = 0, \tag{2.2}$$

respectively. In these equations u is the fluid flux density, S_s is pore space occupied by steam and $S_s = 1 - S_w$. Conservation of energy has a similar form of (rate of gain)+(net outflow)=0 and for single- and two-phase flows is expressed as

$$\frac{\partial}{\partial t}[(1-\phi)\rho_m U_m + \phi\rho U] + \nabla\cdot(uH + \kappa\nabla T) = 0 \tag{2.3}$$

and

$$\frac{\partial}{\partial t}[(1-\phi)\rho_m U_m + \phi S_w\rho_w U_w + \phi S_s\rho_s U_s] + \nabla\cdot(u_s H_s + u_w H_w + \kappa\nabla T) = 0, \tag{2.4}$$

correspondingly. In the conservation of energy equations uH terms signify the energy flux transported by the fluid and $\kappa\nabla T$ terms stand for conductive flux density, since κ is the conductivity of the rock matrix. U denotes internal energy. Using the assumption about homogeneity of a porous medium, one can describe flow in the form of the Darcy equation. In the case of single-phase flow it is

$$u = -k\frac{1}{\mu}(\nabla P - \rho g), \tag{2.5}$$

where permeability k is a tensor. When two phases participate in the flow, the equation includes relative permeabilities k_{rp} and velocities v_p for each phase present are written as follows:

$$u_p = -k\frac{k_{rp}(S_w)}{\mu_p}(\nabla P - \rho_p g), \tag{2.6}$$

where $p \in \{water, gas\}$

Using the above-mentioned governing equations along with the instability conditions, Horne arrives at a conclusion that any system of a particular shape has a preferred solution. At this solution the region of interest experiences the maximum heat transfer. Another important result of his research is that the character of instability in the system depends both on the equation of motion and presence of boundaries (uniformity or non-uniformity of heating). Thus, characterization of natural convection pattern and taking into account the effects boundaries might be valuable in determining the best development strategy for a given geothermal reservoir.

2.2.1 Rayleigh Number

In addition to these key governing equations, in their experiments and numerical simulations the researchers extensively use dimensionless numbers, for example, the Rayleigh number. This number is of particular interest in the study of convection because it relates the rate of fluid convection to the rate of diffusive transport (Schubert and Straus 1978). The Rayleigh number has two definitions corresponding to flat and inclined porous media. For flat systems it is defined as

$$Ra = \frac{k\rho^2 c\gamma\Delta T g h}{\mu\kappa}. \tag{2.7}$$

In this equation γ is the thermal expansivity of the fluid, k is permeability of the porous medium, g is an acceleration due gravity, c is fluid's specific heat, h is a height of the system's square cross-section, ΔT is a change in temperature, μ is the fluid's viscosity and κ is the average thermal conductivity of the fluid and the rock matrix. The value of the Raleigh number indicates if conditions favorable for convection have been reached. Specifically, when $Ra > 4\pi^2$ (here $4\pi^2$ is the critical value derived from a solution with infinite dimension of length) due to nonuniform heating and/or compositional heterogeneities (for instance, changes caused by mixing with gas or salt), the investigated system becomes unstable and convection cells start to form. A typical fluid density change due to natural convection is about 1 percent.

While valid for flat-lying systems, the above-mentioned definition of the Rayleigh number cannot be applied to inclined porous media. For cases when a reservoir has a non-zero dip, a slightly modified formula should be used (Nield and Bejan 2006):

$$Ra = \frac{k\rho^2 c\gamma \Delta T g L \sin\theta}{\mu\kappa}. \tag{2.8}$$

Here the height of the system h is substituted by the length multiplied by sin of the dip $L\sin\theta$. This subtle change in the formula also affects calculation of the critical Rayleigh number. For inclined systems it becomes $4\pi^2\sin\theta$ implying that in dipping reservoirs convection starts to dominate conduction at relatively small Ra values.

2.3 Coupled Convection in Flat and Inclined Systems

After this description of natural convection, the idea of coupled convection widely used in this study should be introduced in more detail. Coupled (or engineered) convection is a phenomenon of mass and energy transfer across the reservoir caused by combined effects of natural and forced convection. Forced convection is usually a result of fluid production/injection via wellbores or sometimes referred as hydraulic conditions that are imposed externally (Sorey 1979). This type of convection is not an exotic idea for either geothermal or oil and gas gas industries. In fact, the process known as displacement (for instance, displacement of hot formation geofluid with cold re-injected one) is forced convection since the fluid's velocity is a function of potential, but not of the reservoir's temperature distribution. Numerical simulations provided later in this thesis show that the presence of dip has a positive effect on heat recovery with coupled convection and both types of convection are more pronounced in inclined geothermal systems.

2.4 Compositional Changes Due to CO_2 Injection: Potential Benefits and Obstacles

Natural and forced convection, however, is not the only drive mechanisms that might cause energy transfer across the region of porous medium. Under certain conditions density differences due to compositional changes, for instance mixing with supercritical CO_2, also can establish convection in fluid. Thus, the review of literature about effects of CO_2 injection into brine or water and compositionally-induced convection is important for several reasons. First, it might provide an insight on if the gas introduction can improve heat transfer to the producing wellbore. Second, it will investigate the optimal injection well placement that allows to avoid interference with geothermal development. Final, the review might tell about potential problems with secure sequestration of CO_2 in convection dominated reservoirs.

In the last decade the concern about greenhouse gases emission into the atmosphere and possibility of global warming induced intense research targeted at geologic sequestration of carbon dioxide. While the majority of articles on the subject are focused on conditions under which the supercritical gas stops migrating underground, the CO_2 sequestration literature produced one interesting by-product – an investigation of CO_2–density–driven convection in geologic formations. This phenomenon is considered undesirable for secure CO_2 storage in natural porous media and is currently scrutinized by a number of scientists with laboratory experiments and numerical simulations.

Kneafsey and Pruess (2009) looked into a problem of CO_2-induced convection in brine and visualize the convective fingers with transparent Hele-Shaw cells as well as TOUGH2 numerical simulator. Because the authors were mainly concerned with calibration of their software tools against their laboratory experiments, so far they modeled only the case when CO_2 interacts with the brine at atmospheric pressure and temperature without any porous medium present. Following up the study by Garcia (2001) who found a 0.1-1 percent increase in aqueous phases density due to CO_2 dissolution, Kneafsey and Pruess verified that CO_2 injection leads to gravitational instability in the system and triggers convective fingering under some conditions.

Farajzadeh (2007) also investigated the effect of CO_2 injection into a porous medium. Their experimental and numerical analysis confirmed that dissolution of CO_2 did enhance thermally-driven convection and that the effect became more pronounced with increasing Rayleigh numbers. In addition to these findings, the authors established that initially for all Rayleigh numbers greater than $4\pi^2$, the CO_2 propagation front moves as a square-root function of time. Later this function becomes linear and fingering continues until the convection stops. For higher Rayleigh numbers, however, transition to the linear function happens faster than for lower. This is an important observation, because the magnitude of the Rayleigh number for this project's model might predict if density-driven convection is going to persist for a long period of time.

The last article to be considered in this section is Pruess and Zhang's (2008) investigation of dissolution, diffusion, and convection effects which occur during CO_2 sequestration in deep saline aquifers. Using TOUGH2 the authors demonstrated that initially after injection of supercritical CO_2 into the reservoir dissolution of the gas in brine is insignificant. As a result, due to its low density and action of the buoyancy force CO_2 tended to flow upward, creating a plume and accumulating under the caprock. Later molecular diffusion removed CO_2 from the sharp interface between the brine and the supercritical gas. Though slow by its nature, this effect became substantial when dense, CO_2-enriched brine started to sink. The negative buoyancy force resulting from CO_2 dissolution launched density-driven convection. Thus, in this thesis low initial impact of density-driven convection should be expected. Understanding this, it might be beneficial to inject CO_2 away from the producer. Such arrangement will take advantage of thermal convection near the wellbore and give more time to a CO_2 plume to sink and enhance density-driven convection.

2.5 Modeling Methods and Tools

Before we can claim that characterization of natural convection provides advantages for subsequent heat extraction and recommend it for industrial application, its physical and commercial viability must be confirmed with numerical simulation on a number of possible development scenarios. This project used the software program TOUGH2 Version 2 to simulate the behavior of a number of potential geothermal reservoirs in quiescent state and in cases of geofluid withdrawal and CO_2 injection. The choice of TOUGH2 is not accidental, because the program was designed specifically for modeling of multiphase and multidimensional flow of fluid mixtures in porous and/or fractured media. Developed under support of the US Department of Energy, this product underwent several decades of testing on various academic and industrial projects, which indicates its robustness, reliability, and flexibility (Pruess et al. 1999).

Pruess et al. (1999) provide a detailed description of this software product and types of problems that it can solve in the report. Using the assumptions about space continuum and local thermodynamic equilibrium, TOUGH2 solves the governing equations of mass and energy balance as well as advective mass and heat fluxes. The authors write a general form of material and energy balance equation as follows:

$$\frac{d}{dt}\int_{V_n} M^{\alpha} dV_n = \int_{\Gamma_n} F^{\alpha} \cdot n d\Gamma_n + \int_{V_n} q^{\alpha} dV_n. \tag{2.9}$$

In this formula V_n is a volume chosen for study and Γ_n is the surface which bounds the control volume. M signifies mass or energy per unit volume, F is mass or heat flux, q is sinks and/or sources, α stands for individual components of the system. Thus, to obtain mass balance, one should put mass accumulation term into the general equation as:

$$M^{\alpha} = \phi \sum_{\beta} S_{\beta} \rho_{\beta} X^{\alpha}_{\beta}, \tag{2.10}$$

where β is a phase, S is saturation, ρ is density, and X^{α}_{β} is fraction of component α in phase β. Similarly, for heat we have:

$$M^{NK} = (1-\phi)\rho_R C_R T + \phi \sum_{\beta} S_{\beta} \rho_{\beta} u^{\alpha}_{\beta}, \tag{2.11}$$

where N_K is number of components, ρ_R is rock density and C_R is its specific heat, T is temperature, and u is specific internal energy. Mass and heat fluxes are modeled in TOUGH2 according to these formulae:

$$F^{\alpha}_{adv} = \sum_{\beta} X^{\alpha}_{\beta}(-k\frac{k_{r\beta}\rho_{\beta}}{\mu_{\beta}}[\nabla P_{\beta} - \rho_{\beta} g]) \tag{2.12}$$

and

$$F^{NK+1} = -\kappa \nabla T + \sum_{\beta} H_{\beta} F_{\beta}, \tag{2.13}$$

where κ is thermal conductivity and H is specific enthalpy of a phase.

In addition to these governing equations, TOUGH2 solves equations of state (EOS) that represent thermophysical properties of fluids. For the cases of heat harvesting with zero net mass withdrawal EOS1 is a suitable option. This equation of state handles thermodynamic properties of water (such as density and internal energy) with experimental accuracy in the broad region starting subcooled water before 350℃ up to superheated steam. Because the conditions of interest fall into the subcooled region. In additional to that, in the case of single phase it requires minimum input – initial pressure and temperature.

For modeling heat extraction with simultaneous CO_2 injection this study uses another TOUGH2 EOS module called EWASG (WAter-Salt-Gas). This equation of state is of particular interest in this project, because it handles fluid properties for mixtures of water, solid salt, and a non condensible gas (NCG), for example, CO_2, air, CH_4, H_2, or N_2. EWASG uses Henry's law to simulate gas dissolution in the aqueous phase that depends both on temperature and salinity. This option is very important for modeling geothermal systems with non uniform brine salinity. This EOS module also implements dependence of fluid density, viscosity, enthalpy, and vapor pressure on salinity.

Although TOUGH2 has several EOS modules that handle flow of CO_2 and water, only EWASG is suitable for the current problem. This EOS module simulates flow under conditions of interest. More specifically, EWASG's temperature range is from 100℃ to 350℃, pore pressures are as high as 80 MPa, salt mass fraction up to saturation, and CO_2 partial pressures are from none to 10 MPa. In addition to this, EWASG module can simulate the flow without presence of a non-condensible gas and with permeability reduction.

As explained by Battistell, Calore, and Pruess (2007), the EWASG module solves equations for four primary variables: total pressure P, salt mass fraction X^{salt} (or solid saturation for two-phase flow S^{salt}), non-condensible gas mass fraction X^{NCG} (or gas phase saturation for two-phase flow S^{NCG}), and temperature T. The EOS verifies if the switch from liquid to two-phase conditions has occurred with the following inequality:

$$P < P_{boil}(T, X_L^{salt}, X_L^{NCG}), \tag{2.14}$$

where boiling pressure is given by:

$$P_{boil} = P_{bsat}(T, X_L^{salt}) + P^{NCG}(T, X_L^{salt}, X_L^{NCG}). \tag{2.15}$$

P_{bsat} signifies brine's saturation pressure and NCG's bubbling pressure and P^{NCG} is from Henry's law. EWASG allows for a solid phase to evolve in the system, the following condition checks if salt starts to appear:

$$X_L^{salt} > X_{sol}^{salt}(T), \tag{2.16}$$

where $X_{sol}^{salt}(T)$ is a salt mass fraction soluble at a given T. EWASG calculates liquid's thermophysical properties according to assumptions that density and viscosity of the liquid are equal to those of brine and, thus,

$$\rho_L = \rho_{brine}(P, T, X_L^{salt}), \tag{2.17}$$

$$\mu_L = \mu_{brine}(P, T, X_L^{salt}), \tag{2.18}$$

$$H_L = (1 - X_L^{NCG})H_{brine}(P, T, X_L^{salt}) + X_L^{NCG} H_L^{NCG}(P^{NCG}, T). \tag{2.19}$$

This EOS module uses Haas' correlation to compute brine density which produces accurate results for temperatures between 75℃ and 325℃. Enthalpy of brine (or water) is determined according to the correlation of Michaelides with minimum error between 100℃ and 350℃. Battistelli's report on EWASG's capibilities also contains detailed descriptions and references to correlations for calculating enthalpy, viscosity, and density of non-condensible gases that are omitted in this literature review for the purposes of brevity.

2.6 Additional Considerations on Power Conversion and Electricity Generation

Although on surface power conversion and economic analysis is not an integral part of this thesis, in conclusion of this chapter some general overview of how raw thermal energy can be converted into electricity is necessary. The detailed report on geothermal potential of the US (MIT 2006) provides a thorough description of present day challenges and advances in electricity generation from geothermal energy. For low-enthalpy geofluids, such as those produced from sedimentary geothermal systems, the report recommends binary energy conversion system with working fluid isobutane or R-134a. Binary systems like this are organic Rankine cycles for which net power output (in kW) can be estimated with the following correlation:

$$W = (0.098701 - 0.0039645T_1)q\Delta T_2, \tag{2.20}$$

where W is net power output adjusted for thermal energy availability and turbine efficiency (obtained from the analysis of several working binary plants), T_1 is fluid inlet temperature, ΔT_2 is difference between temperature of fluid leaving the plant and inlet temperature (T_2 is 35 ℃ in most plant designs), q is geofluid flow rate. Thus, if the geofluid with temperature of 135 ℃ is delivered to the cycle at a flow rate of 20 kg/s, the power output is about 873 kW. Alternatively, one can calculate net power output by applying thermal energy availability and turbine efficiency coefficients to raw thermal energy output from the producer well. It is also important to mention that, in addition to energy conversion system, economic attractiveness of a geothermal project is a function of the aquifer's volume. As Griggs (2004) suggests at least 1 cubic kilometer volume of fluid saturated rock is required to consider economic geothermal development.

Although there are obstacles in commercialization of geopressured geothermal resource, there are examples of successful pilot projects that inspire this study. One such project is Pleasant Bayou geopressured reservoir in southeast Texas. This reservoir is many aspects (petrophysical and geometric) similar to the described above the Camerina A sand. The pilot 1MW plant was run from 1989 to 1990 and generated 3,445 MWh over 121 days at an average power output of 1,200 kW (Riney 1992).

Chapter 3

Natural Convection Modeling

This chapter discusses an experimental design for natural convection modeling, juxtaposes quiescent systems initialized with and without bounding layers, and examines if natural convection can be an effective heat drive mechanism.

3.1 Modeling Design

As was mentioned in the previous chapter, any geopressured geothermal aquifer undisturbed by heat extraction or oil and gas production in the past has a natural convection pattern in-place that creates a certain temperature profile. (Hanor 1987) modeled natural convection on the large scale across bedded sediments of the Gulf of Mexico region. This work opened a venue for research about natural convection in individual units or aquifers in the same geographic region that this thesis is concerned with. In order to see the benefits of initializing geomodels with proper geothermal gradient and running the quiescent period, a number of 2D TOUGH2 simulations are run with varying geometries and petrophysical properties. Only one property is varied at a time and for each case Rayleigh number and its critical value is calculated (Appendix D: Natural Convection Modeling summarizes all cases in a table). All geomodels have three layers of rock: the top and the bottom ones are impermeable bounding layers with infinite heat capacity and the middle one is the porous medium. Initialization script (Appendix E: Awk Initialization Script provides the code) assigns temperature value to each grid block (including bounding layers) according to the chosen geothermal gradient.

3.2 Quantitative and Qualitative Description on Natural Convection Pattern

3.2.1 Rayleigh Number

From Appendix D tables pertaining to quiescent system modeling it is clear that dip controls the primary heat transport. For geomodels with dips equal to zero or almost zero values of Ra are significantly lower than the critical value, indicating that these systems are conduction dominated. Presence of even small dips, however, amplifies the effects of other properties, such as permeability, length, and thickness, and makes convection the major energy transfer mechanism.

3.3 Effect of Bounding Layers and Natural Convection

To know the primary heat transport (conduction or convection) beforehand is valuable for future production planning, but not sufficient for adequate resource estimation and developing of production strategy. In addition to the Rayleigh number, one needs to know the approximate shape of the natural convection pattern, the span of the quiescent period during which convection stabilizes, and the effect of bounding layers on the reservoir's temperature profile. This section provides specifics on these three aspects.

Nield and Bejan (2006) outlined problems with computing and examining convection patterns in inclined porous media and drew attention to the possibility of multiple solutions for the same geometries. Keeping in mind these complications as well as limitations imposed by 2D simulations and software tools for visualization, we conclude that for the selected geomodels with slab-like geometry the convection pattern looks approximately unicellular. Figure 3.1 displays a convection pattern on a coarse grid.[1]

The next consideration in natural convection characterization is duration of the quiescent period for a geothermal system. In this thesis, *quiescent* means a reservoir which has no *artificial* injection or production. Because computational efficiency is always important in numerical simulation, the quiescent period should be the shortest time span after which no significant change in convection pattern occurs. To establish this time period, we consider cases with moderate but different Ra and estimate the time span after which temperature and aqueous phase flow in each grid block changes negligibly. Cases 2 and 8 from the experimental design are suitable for this analysis and were run for 1 million years as quiescent systems. Appendix E: R Code for Quiescent Period Calculation in Geothermal Systems provides details of how the quiescent period of 1,000 years is obtained. Because the mean of difference of aqueous phase flow values between 1,000 and 10,000 years comprises less than 0.1 percent of mean of initial aqueous phase flow values in both cases, the change in aqueous phase flow in each grid block is not significant after 1,000 years of natural convection. The same holds true if temperatures are analyzed instead of aqueous phase flow. The results of temperature calculations are omitted for brevity.

To demonstrate how the natural convection pattern stabilizes, the previously used $5\times1\times5$ geomodel is kept quiescent for one million years. Figure 3.2 compares vector plots of aqueous phase flow after 1 second, 1,000 years and 1 million years. There is little visual or quantitative difference after 1,000 years.

The final aspect of natural convection modeling that requires discussion in this section is the effect of bounding layers on the reservoir's temperature profile. Impermeable top and bottom bounding layers with infinite (or very large) rock heat capacity simulate low permeability (for instance, shale) layers that allow heat, but not mass transfer in and out of the reservoir. Bounding layers with large heat capacity produce the smooth temperature profile illustrated in the Fig. 3.3.

[1]For all geomodels in this thesis length is in x-direction (left-right), width is in y-direction (in-out of the page), and height is in z-direction (down-up). Apparent visual dip is used to denote dipping systems, though the apparent dip angle does not necessarily correspond to the modeled dip.

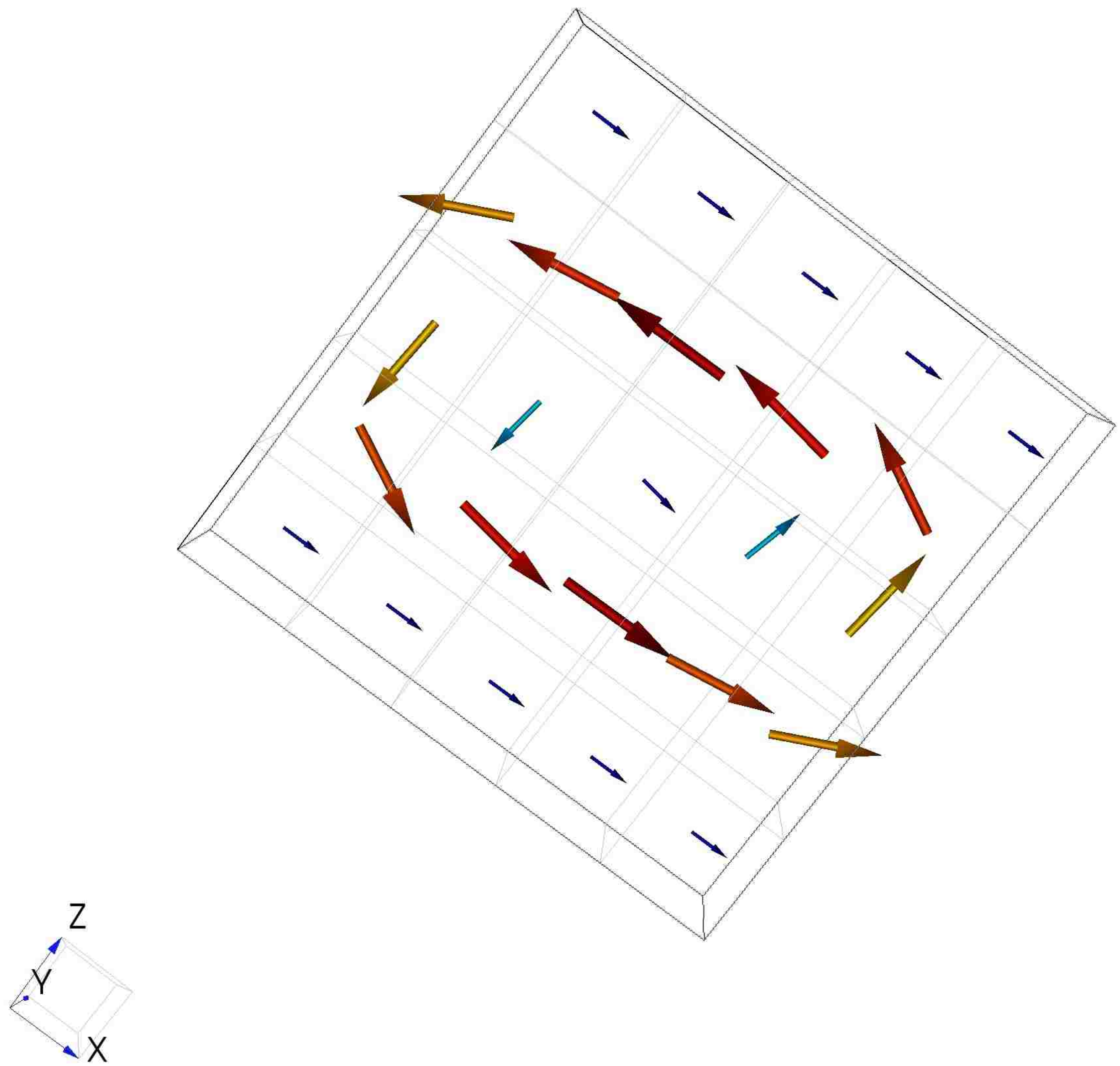

Figure 3.1: Vector plot of aqueous phase flow (kg/s) for 5×1×5 blocks (500 m in x-direction, 100 m in y-direction, and 500 m in z-direction) geomodel dipping at 45 degrees with top and bottom bounding layers of infinite heat capacity. Pattern snapshot is taken after 1,000 years of quiescent period, modeled in TOUGH2 and visualized with PetraSim software. Heat is conducted into the bounding layers high in the reservoir, and into the reservoir at greater depths. Length and color of the vectors reflect the magnitude of mass transfer. The range is from short vectors with cold colors to long ones with warm colors. For this snapshot the range is from 0 to 0.00003 kg/s.

In this plot taken after 1,000 years quiescent period, temperature contours appear near–horizontal (if there is no vertical exaggeration), and their slight curvature is due to natural convection in the reservoir's geofluid. Figure 3.4 shows upward flow of heat on the top

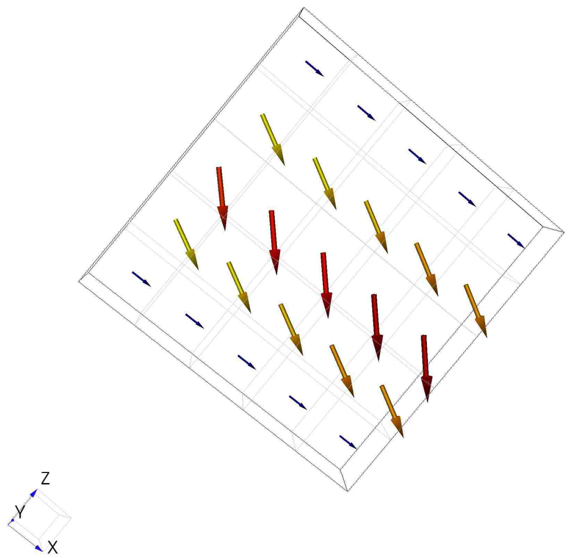

(a) 1 second.

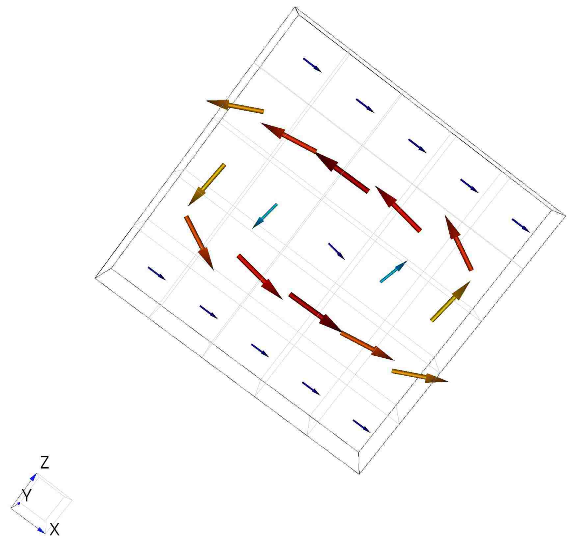

(b) 1,000 years.

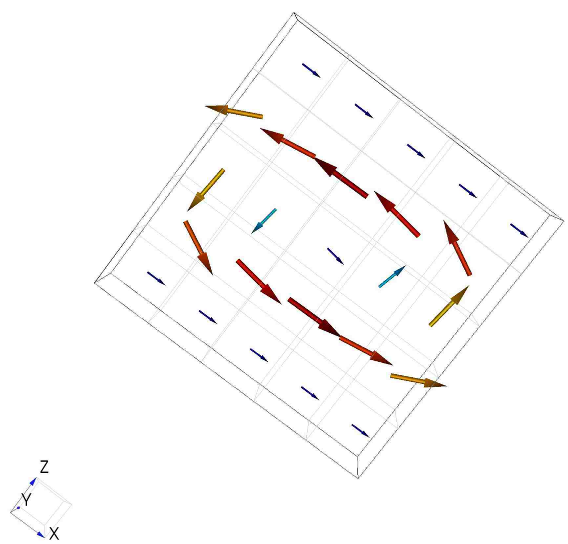

(c) 1 million years.

Figure 3.2: Vector plots of aqueous phase flow (kg/s) for 5×1×5 blocks (500 m in x-direction, 100 m in y-direction, and 500 m in z-direction) geomodel with top and bottom bounding layers of infinite heat capacity. Pattern snapshots are taken after 1 second, 1,000 years and 1 million years of the quiescent period. Visually the pattern stablizes after 1,000 years.

boudary that pulls contours downdip, and vice versa on the bottom.

When the bounding layers are not included, and the model is run for the same quiescent period of 1,000 years, the range of temperatures decreases, and with lesser natural convection, the temperature contours are nearly planar and simpler in structure. (Fig. 3.5).

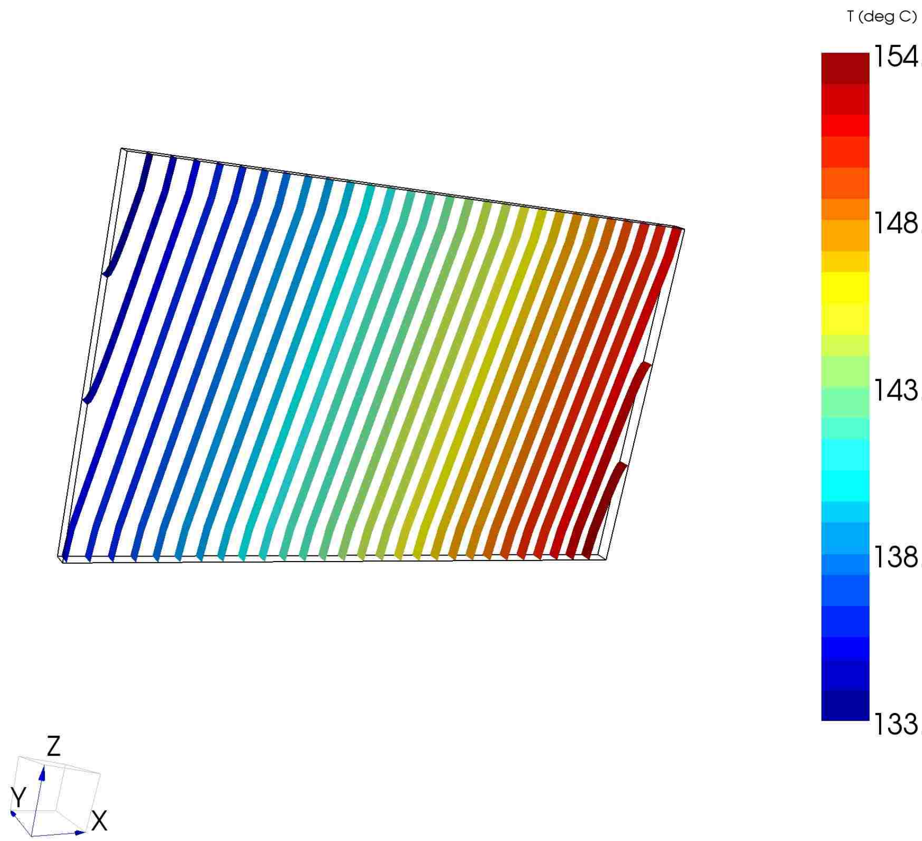

Figure 3.3: Temperature profile for a 4000×100×100 m (4000 m in x-direction, 100 m in y-direction, and 100 m in z-direction) model with the bounding layers, the vertical gradient of 18 ℃/km and 15 degrees dip (plotted with the 20 fold exaggeration in z-direction). The bounding layers produce equally spaced temperature contour lines expected for a medium with uniform petrophysical properties.

Even though the reservoir has uniform petrophysical properties, the range of temperatures without bounding layers is 6℃ less than in the previous case and the contours are not equally spaced. Because the bounding layers give a wider, evenly spaced, and more realistic temperature profile (realistic in a sense that any Gulf of Mexico geopressured aquifer is bounded by other formations that conduct heat in and out of the reservoir), all production cases discussed below are initialized and kept quiescent for 1,000 years. The last illustration in this section (Fig. 3.6) shows the interdependence of the Rayleigh number and variance of temperature:

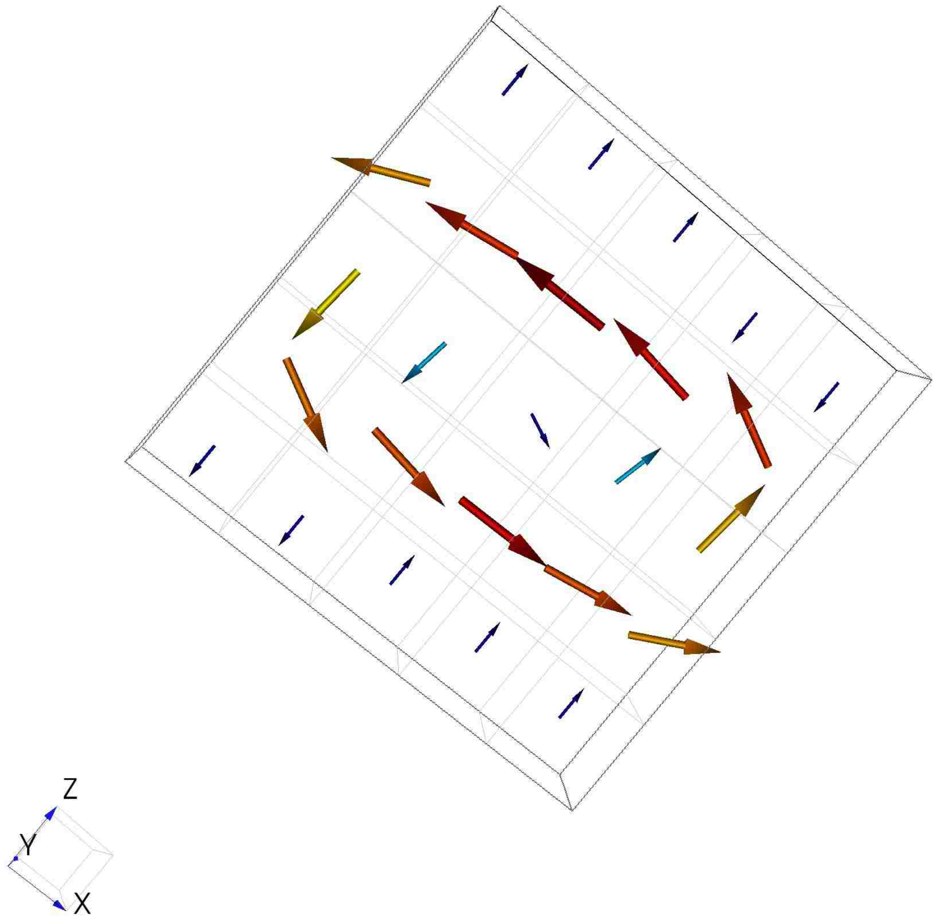

Figure 3.4: Vector plot of flow of heat for 5×1×5 blocks (500 m in x-direction, 100 m in y-direction, and 500 m in z-direction) model with bounding layers and 45 degree dip. The snapshot is taken after 1,000 years and demonstrates heat flow out of the reservoir on the top and into on the bottom. Length and color of the vectors reflect the magnitude of heat transfer. The range increases from short vectors with cold colors to long ones with warm colors. For this snapshot the range is from 0.06 to 1.68 W per m^2.

3.4 Natural Convection Pattern for Camerina A

The literature survey from the previous chapter provides the petrophysical and thermodynamic properties for Camerina A sand geomodel (Section 2.1.1 gives the details). While some of them, for instance formation temperature, permeability, and thickness can be incorporated into the model as they are, others require averaging. Porosity given in the range between 9 and 31 percent and dip from 1.2 to 28 degrees need adequate average values that would not alter the output beyond the acceptable error range.

In order to assign an average value to porosity, let us demonstrate that energy output is not sensitive to variations in porosity, everything else being equal. For this purpose a simple

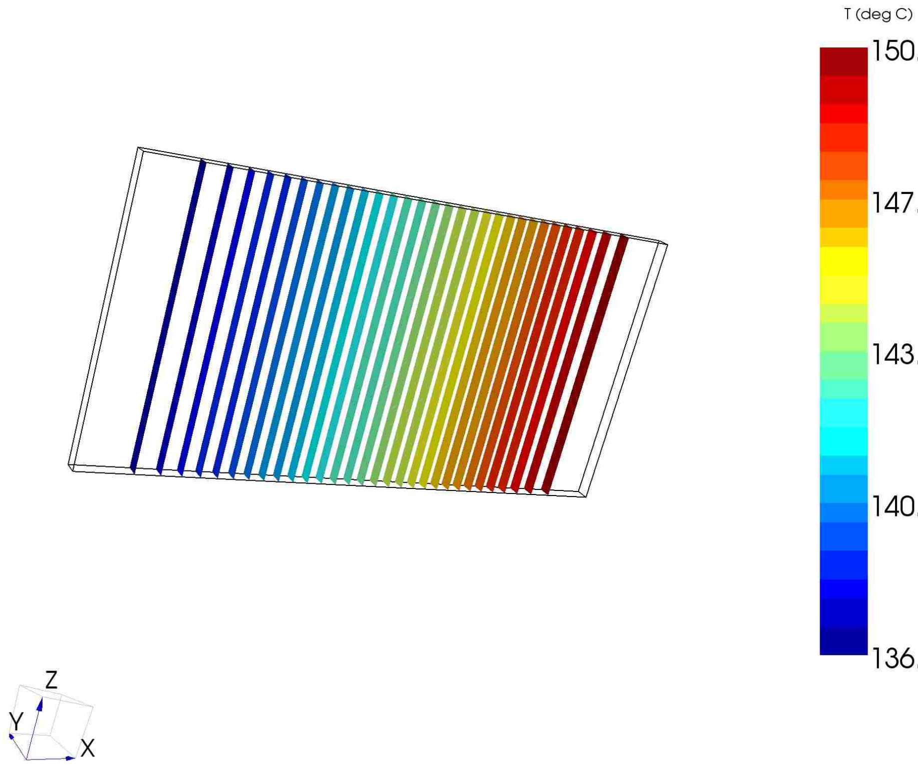

Figure 3.5: Temperature profile for a 4000×100×100 m (4000 m in x-direction, 100 m in y-direction, and 100 m in z-direction) model with the vertical gradient of 18 ℃/km and 15 degrees dip initialized without bounding layers (plotted with the 20 fold exaggeration in z-direction). The temperature contour lines are not equally spaced and the range of temperatures is less than in the case with the bounding layers.

2D TOUGH2 model (Fig. 3.7) is run for porosity in the set (0.05, 0.1, 0.15, 0.2, 0.25, 0.3).

The analysis of heat extracted values shows that the mean is 8.858×10^{14} and the standard deviation is 1.128×10^{13} which is less than 2 percent (Appendix D gives further details). Thus, variability in porosity does not influence energy output significantly, and for both natural and coupled convection simulations a porosity of 20 percent will be used. The range of dips presents an averaging problem, because it has strong influence on Ra and, therefore, energy transfer across the system. Keeping in mind this complication and that in the Northern Gulf of Mexico region high dips cannot be sustained for the entire length of the aquifer, it is appropriate to assume Camerina A sand's dip value between 2 and 5 degrees.

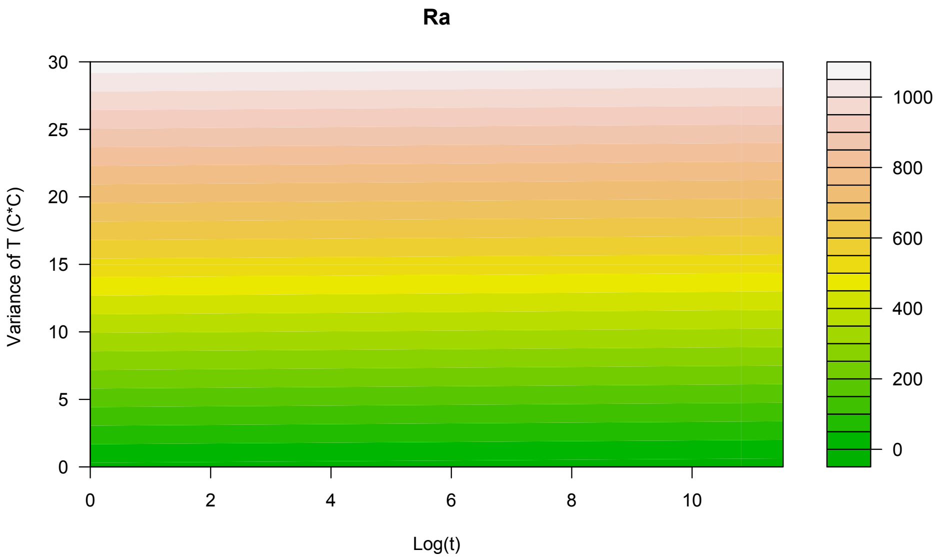

Figure 3.6: Contour plot of variance of temperature and logarithm of time (log(t)) *vs.* Ra. The higher *Ra* correspond to higher variances. The plot's legend represent color coded *Ra* values.

3.5 Natural Convection as Heat Drive Mechanism: Wellbore Cooling

Now that the concept of natural convection in geothermal reservoirs is developed quantitatively and qualitatively, it is necessary to see if this heat transport can be used to extract significant amounts of energy. For this purpose let us model the system of interest with high and varying permeability, since this petrophysical property controls how fast the fluid migrates within the porous medium. In addition to high permeability, let us use only one aquifer configuration that ensures one of the highest *Ra* and the most vigorous natural convection (for precise properties see Appendix D, Experimental design Case 12). Figure 3.8 graphically summarizes the wellbore cooling design and the position of the horizontal heat extractor in the large unicellular convection pattern. In this heat extraction design, natural convection is augmented by chilling, with the goal of inducing sufficient convection to obtain commercially viable heat fluxes to the chilled well.

This heat harvesting approach requires only one horizontal well through which a refrigerant is circulated from the surface to the formation and back to a facility with power generation equipment. For low-enthalpy geothermal systems the refrigerant would be a low boiling point fluid such as isobutane or R-143a (in this case the boiling point is 50°C), and the turbine would be powered by an organic Rankine cycle. For the convenience of energy balance calculations, bounding layers are excluded from the model for 30 years of heat extraction. The initialization step, nevertheless, is exactly the same as for regular geofluid production cases. The range of permeabilities is rather high for geopressured geothermal aquifers found in the Gulf coast, but not impossible for unconsolidated well-sorted sediments. The set

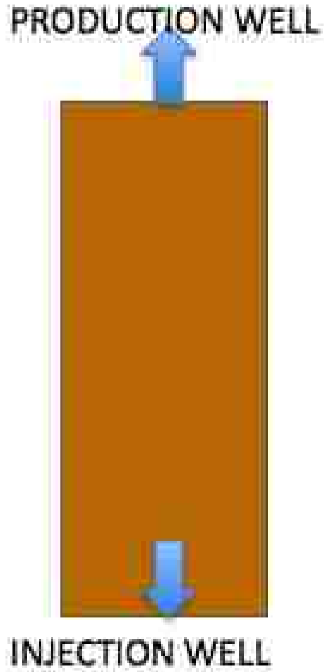

Figure 3.7: Schematic illustration of 2D TOUGH2 model 100×100×1000 m (100 m in x-direction, 100 m in y-direction, and 1000 m in z-direction) with a producer on top and an injector on bottom. Production and injection rates are 10 kg/s, rock compressibility - 2×10^{-8} 1/Pa, pressure of 34.5 MPa, initial temperature equal to 135℃, permeability is 100 mD and porosity independent.

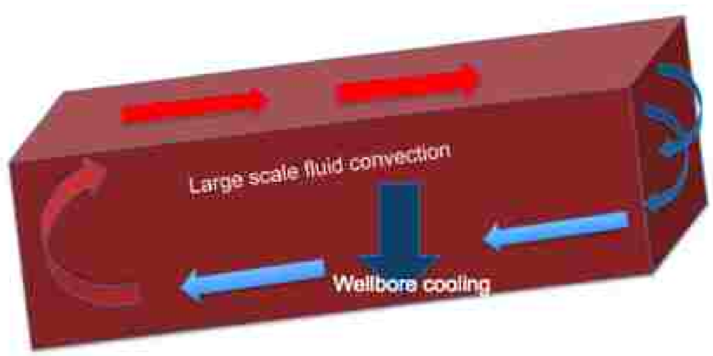

Figure 3.8: Conceptual arrangement for geothermal development via wellbore cooling. The plume of chilled water descending from the heat sink is intended to augment natural convection and accelerate heat recovery.

of permeabilities used includes 1, 10, and 100 darcies (Panda and Lake 1994). Although these permeabilities are higher than expected for Gulf of Mexico geopressured aquifers, examination of convection at such extreme values will provide insights into heat transport in geothermal systems. Using the relation proposed by Panda and Lake (1994) for permeability estimation, we can deduce approximate particle size in simulated porous media:

$$k = \frac{D_p^2 \phi^3}{72\tau(1-\phi)^2}, \tag{3.1}$$

where D_p is a particle diameter, ϕ is porosity, and τ is tortuosity of the porous medium. Solving for D_p^2, we obtain:

$$D_p^2 = \frac{72k\tau(1-\phi)^2}{\phi^3}. \tag{3.2}$$

Dullien (1979) suggests that for typical sandstones it is acceptable to use τ=2 and, thus, the particle size table based on Wentworth grain scale for permeabilities of 1, 10, and 100 darcies follows:

Table 3.1: Particle sizes for given values of permeability

	permeability (m^2)	porosity	particle size (mm)	name	type of sediment
1	10^{-12}	0.20	0.0107	silt	siltstone
2	10^{-11}	0.20	0.0240	fine sand	sandstone
3	10^{-10}	0.20	0.0758	fine sand	sandstone

For the three simulation runs the geomodels with the highest *Ra* are selected to amplify the effect of energy transfer due to natural convection. 2D TOUGH2 numerical simulations use models with extents of 4000 × 100 × 200 m systems dipping at an angle of 15 degrees. Because the bounding layers complicate energy balance calculations, the results are more qualitative and can be represented as temperature profiles after 30 years of heat harvesting in the Fig. 3.9.

The system with permeability of 100 darcies produces the greatest amount of heat. Statistical analysis of temperatures after 30 years yields an interesting trend. The mean reservoir temperature is still near initial temperature (139.3℃ *vs.* 135℃) for the 1 D case (left, Fig. 3.9), whereas for 10 D (center, Fig. 3.9) the average reservoir temperature falls to 121.1℃, and the 100 D case (right, Fig. 3.9) draws down to 95.4℃ (Appendix E: R Code for Wellbore Cooling Cases provides details of the analysis). If differences between temperatures are calculated for each grid block, the results are even more striking: some cells have temperature difference between the first and the third systems approaching 100℃. Thus, if systems with very high (> 10 D) are found, wellbore cooling might be a viable option for heat extraction without withdrawing any fluid from the subsurface.

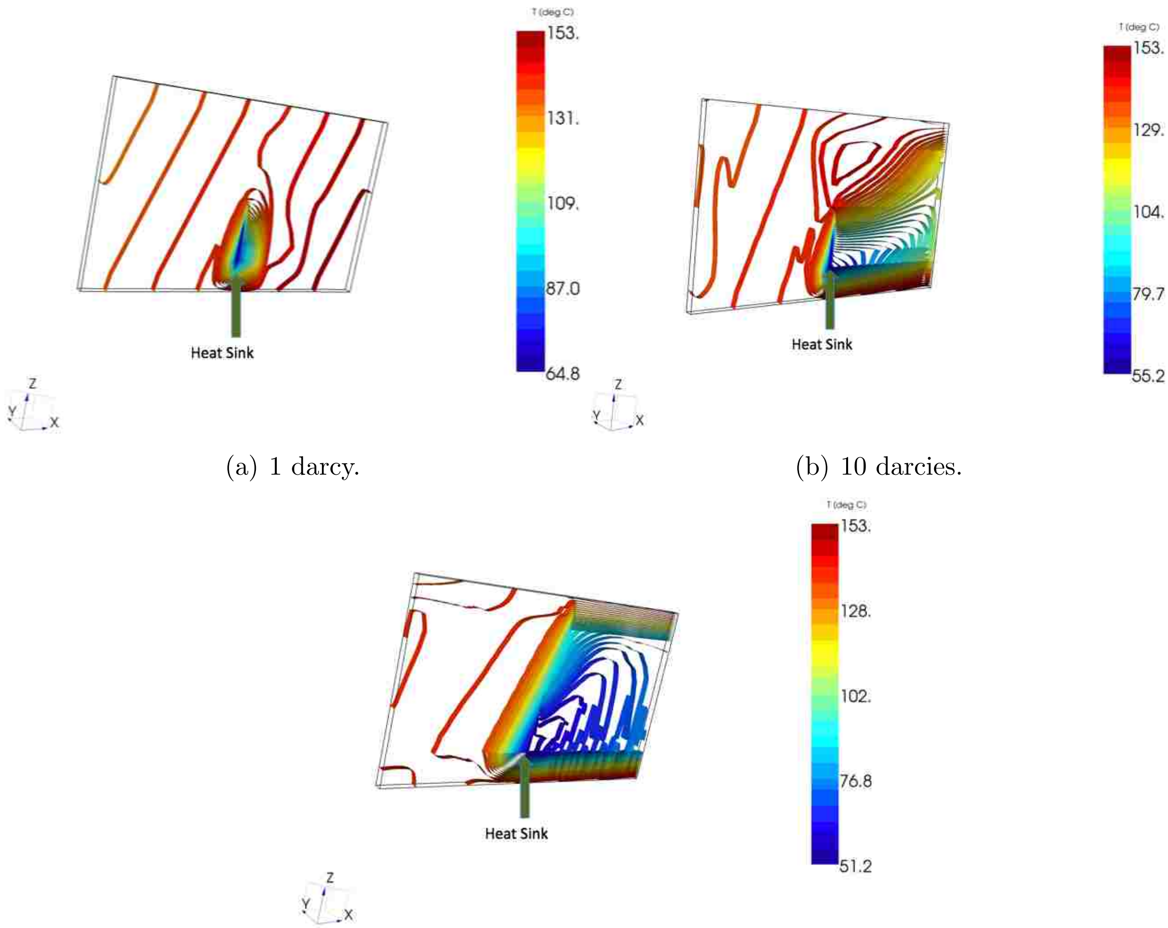

(a) 1 darcy.

(b) 10 darcies.

(c) 100 darcies.

Figure 3.9: Temperature distributions after 30 years of wellbore cooling at 50℃ for the systems with permeabilities of 1, 10, and 100 darcies. For the "low" permeability 1 D case, an isolated plume of chilled water descends from the heat sink, but no large–scale convection cells are formed. As permeability increases heat sweep becomes more pronounced and engages deeper portions of the reservoir.

Chapter 4

Coupled (or Engineered) Convection Modeling and Effect of CO_2 Injection

As described in the previous chapters, natural convection has influence on initial temperature distribution in the system of interest, but it is not a powerful enough heat transport mechanism to be utilized for commercial geothermal development in typical hot saline aquifers of the Gulf Coast. Therefore, energy transport due natural convection must be enhanced by forced convection via wellbore production and injection. This chapter describes an experimental design for geofluid production cases with and without simultaneous CO_2 injection.

4.1 Experimental Design for Coupled Convection Production Cases

Because one of the objectives of this study is to find parameters that influence heat recovery the most, a full factorial experimental design with three parameters deemed likely to be influential is selected. Appendix B contains a table with all cases listed. To encompass a realistic range of geometric and petrophysical properties found in the Northern Gulf of Mexico basin, two levels of permeability (100 mD, 1000 mD) and thickness (100 m, 200 m), and three levels of dip (0 degrees, 2 degrees, 15 degrees) are used (Ewing, Light, and Tyler 1984). Other properties used for 2D TOUGH2 simulations are summarized in Table 4.1.

The formation pressure and geothermal gradient (Table 4.1) are lower than they would be expected for the zone of geopressure in the Gulf coast. Gray (2010) suggests that the Camerina A sand, which is a typical sand deposit in the geopressure zone, has a geothermal gradient of 29 ℃/km and formation pressure over 80 MPa. These values, however, are lowered for two reasons. First, the equation of state (EWASG) is less stable for high pressures and temperatures. Second, we seek to compare production cases with and without CO_2 injection. A high initial pressure gets even higher with dip and precludes simulations with CO_2 injection, with available equations of state and for reasonable injection pressures. Thus, to compare energy output from the systems in which only CO_2 injection rate is variable (0 or 10^{-4} kg/s), the initial formation pressure is kept at 34.5 MPa.

In addition to the parameters listed in the table above, each case produces the system at three different injection/production flow rates (0.2, 2, and 20 kg/s per 100 m of well) and examines two production arrangements (regular and reverse). Schematically, these two

Table 4.1: Reservoir properties for 2D simulation runs

Property	Value	Units
initial pressure	3.45×10^7	Pa
initial average temperature	135	℃
porosity	0.20	–
matrix compressibility	2.0×10^{-8}	1/Pa
injection water enthalpy	3.0×10^5	J/kg
rock density	2600	kg/m^3
wet rock heat conductivity	2.0	W/m ℃
reservoir length	4000	m
reservoir width for 2D run	100	m
salinity	0	ppt
geothermal gradient	18	℃/km

designs are illustrated in the Fig. 4.1.

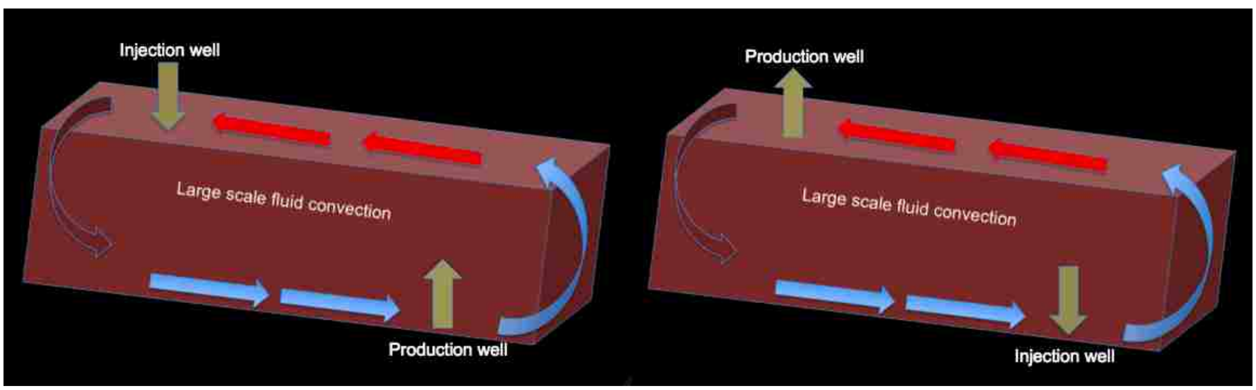

Figure 4.1: Regular (left) and reverse (right) production arrangements. The "regular" arrangement is intended for efficient natural convection.

Regular design places one horizontal production well at the bottom of the reservoir that contains geofluid of the highest enthalpy within the system and re-injects cooled formation fluid at the top. The choice of this location for re-injection is dictated by a couple of reasons including relatively lower formation pressure at the top and the descending part of the large-scale convection loop. As Horne (1975) mentioned in his research on convection dominated systems, placing cool water injection well into a descending stream might provide an increased heat recovery. Reverse design, on the other hand, displaces hot geofluid updip from deeper parts of the reservoir by cool water injection.

The effects of salinity and dissolved gases such as methane are omitted from these models. Methane is excluded because it is not very important economically (Griggs 2004). Correct modeling of salinity variations is complex (Hanor 1987). More specifically, proximity to salt domes and aquifer structure and properties affect the salinity distribution, which is non uniform and may be transient over long time scales. Modeling a realistic salinity profile in addition to temperature distribution would require initialization with salt and fresh water sources, which makes modeling less general and more attached to specific geologic setups. Thus, the flow simulations in this chapter do not include factors for varying salinity and gas fraction.

Appendix D presents the results of 2D simulation runs for all cases listed in the experimental design table. The summary table shows only energy recovered after 10, 20, and 30 years of production with both types of production arrangements, but for each case there are output files with year-by-year values of produced water enthalpy (also consult Appendix D). This detailed output allows calculation the cumulative amount of energy extracted over 10, 20, and 30 years (using an average enthalpy value for each year). Though this is an approximate method to compute energy recovery for the system, it eliminates the problem of calculating heat fluxes in and out of the bounding layers. Because produced water enthalpy varies smoothly and slowly (annual changes of no more than 3 percent), the chosen procedure for energy calculation is sufficiently accurate. The same computation method is applied for cases with CO_2 injection.

4.2 Experimental Design for Coupled Convection and Simultaneous CO_2 Injection

Geothermal reservoir behavior with both heat extraction and CO_2 injection is examined using the the same experimental design as for coupled convection production. The twelve cases with CO_2 injection are initialized, idled and produced similarly to coupled convection cases. However, a horizontal CO_2 injection well is added (Fig. 4.2).

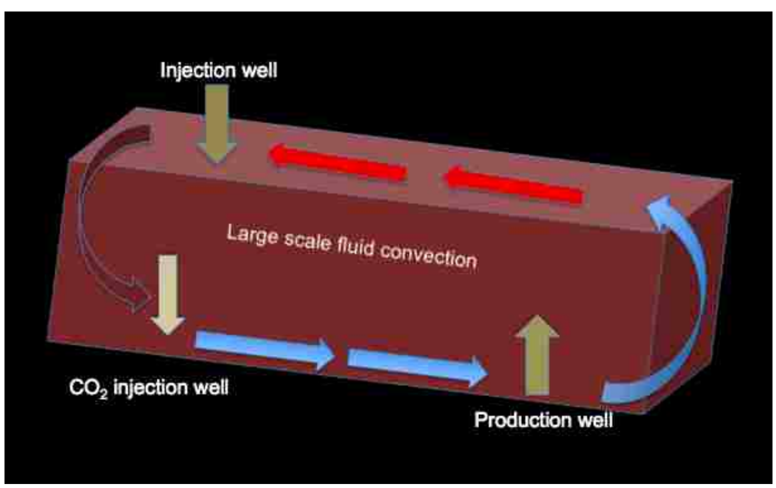

Figure 4.2: Regular production arrangement with CO_2 injection. The CO_2 is injected into the descending branch of the convective loop.

Placement of CO_2 injection well is dictated by the following reasoning. CO_2 injection well should avoid the regions of geofluid production and injection. If the supercritical greenhouse gas injected in proximity of hot water production, we will extract enthalpy of the gas mixture instead of that of the geofluid. This might significantly reduce heat recovery from the reservoir. If CO_2 is injected close to the geofluid injection region, the volume of the injected gas will drop, because formation pressure in this portion of the reservoir would be elevated.

The rate of the supercritical CO_2 injection must also be specified. Because the range of permeability is wide (from 100 to 1000 md), a small injection rate of 0.0001 kg/s is selected. This constant value allows comparing the simulations without introducing another factor and running an additional set of simulations. Now that the conceptual framework is developed and the experimental design is discussed, we analyze results of simulation runs in the following chapter.

Chapter 5

Results

This chapter provides a statistical analysis of energy output from three main suites of simulations, identifies design factors that control energy recovery, and presents illustrative figures and discussion.

5.1 Sensitivity Study

Using an experimental design (Appendix B), three sets of simulations were generated (1) twelve geofluid production cases initialized without the proper geothermal gradient and idle period,(2) twelve geofluid production cases with natural convection in-place at the time of heat extraction, and (3) a set of twelve cases with simultaneous geofluid production and CO_2 injection, initialized with natural convection. The output of interest for all simulation runs is energy extracted after 10, 20, and 30 years of production. These results along with the factors are merged into one dataset and imported into R (Team 2008).

To focus on the most important factors, the dataset is split into subsets by time (10, 20, 30 years) and flow rates (0.2, 2, 20 kg/s) and inspected for correlation. Correlations between energy outputs for 10 and 20 years and 20 and 30 years are 0.999 and 0.998 correspondingly. Correlations between subsets split by production flow rate are 0.999 and 0.997 for 0.2 - 2 kg/s and 2 - 20 kg/s respectively. Therefore, it is possible to reduce the number of factors by analyzing only one subset with energy output after 10 years of production at a flow rate of 0.2 kg/s. All significant factors found for this subset will also be significant for the entire dataset.

Appendix E: R Code for Selecting Model and Plotting with Contour Plot provides an algorithm used to obtain the model with the most significant factors. A stepwise regression run and a subsequent ANOVA test show that dip, convection and their product are the most influential factors:

$$E = D + C + D \cdot C \tag{5.1}$$

where C is a boolean variable indicating wheher the simulation was run with natural convection initialization, D is dip, and E is energy output. Even though this model is a result of the analysis that tries to fit all possible combinations of the factors and outputs the best fit, the multiple R^2 is relatively low (0.57), indicating poor fit. Nevertheless, an ANOVA test confirms that the two factors identified by the stepwise regression are the most significant (Appendix D: Model Fitting contains the R code and output).

To conclude this chapter, one might be interested in observing the combined effect of geometric and petrophysical properties on raw thermal energy output at a high flow rate and after substantial production period of 30 years. Figures 5.1, 5.2, and 5.3 provide three contour plots that illustrate the effect of dip and permeability for the three simulation suites.

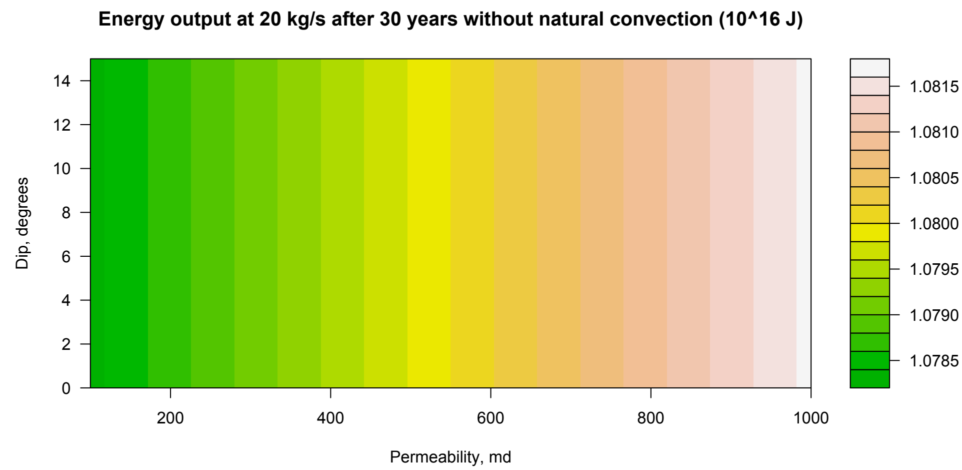

Figure 5.1: Contour plot shows energy recovery in Joules from the systems initialized without natural convection and produced at a rate of 20 kg/s for 30 years. There is no CO_2 injection.

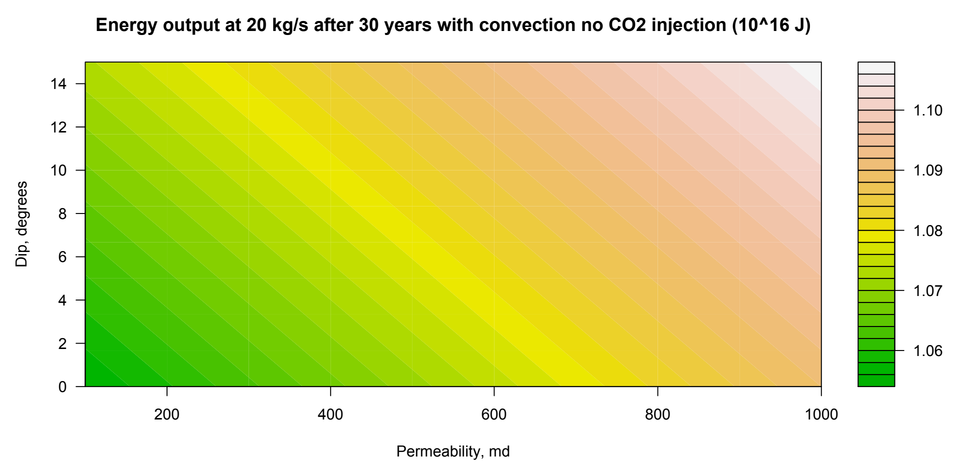

Figure 5.2: Contour plot shows energy recovery in Joules from the systems initialized with natural convection and produced at a rate of 20 kg/s at 30 years. There is no CO_2 injection.

The figure 5.1 shows that the lack of initialization with natural convection fails to capture higher geofluid enthalpy and, thus, higher energy recovery in dipping systems. The last two plots (Figs. 5.2 and 5.3) fully capture this effect There is consistently higher energy output and a stronger combined effect of dip and permeability for the cases with CO_2 injection.

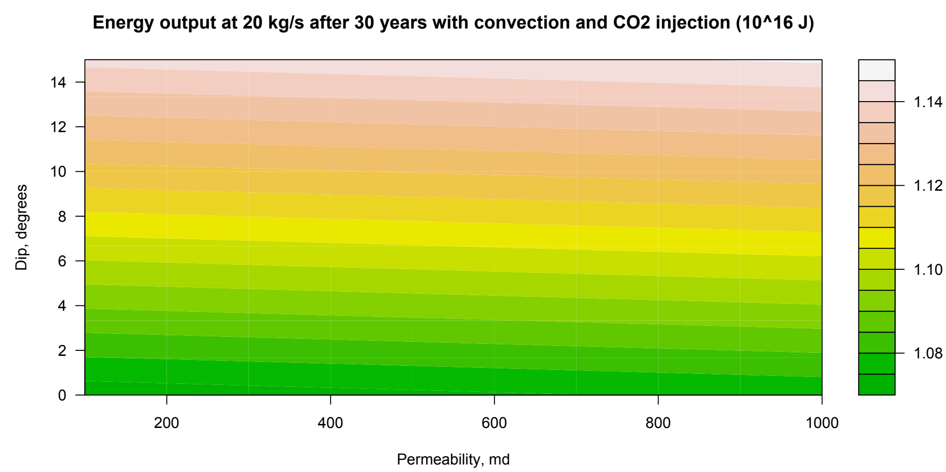

Figure 5.3: Contour plot shows energy recovery in Joules from the systems initialized with natural convection and produced at a rate of 20 kg/s for 30 years. There is simultaneous CO_2 injection.

Chapter 6

Discussion

Now that the results of the simulation runs are analyzed quantitatively, the most significant factors are identified, and the fundamental research expectations are confirmed, it is appropriate to discuss qualitative aspects and implications of this study. This chapter discusses how the obtained results fit into the existing scholarship about geothermal systems and enhance present day understanding of their behavoir.

6.1 Considerations on Production Designs

The analysis of energy output for regular and reverse design based on the subset with natural convection indicates that regular design outperforms reverse with the mean difference of 1.567×10^{12} Joules for the flow rate of 0.2 kg/s after 10 years of production. With a mean energy output of 3.697×10^{13} Joules for this subset, we conclude that on average the regular design extracts about five percent more energy than the reverse. Five percent is an approximate number that is sensitive to dip of the produced system. To visualize how performance of a regular design improves with dip one can examine the relative difference of energy outputs for the cases produced between energy outputs of reverse and regular designs (relative difference is defined as $2(E_{\mathrm{reg}} - E_{\mathrm{rev}})/(E_{\mathrm{reg}} + E_{\mathrm{rev}})$ and calculated here for 0.2 kg/s at 10 years). Increasing dip and thickness make regular design a more attractive production arrangement, as indicated by the positive differences (Fig. 6.1).

This finding substantiates suggestion by Horne (1975) about benefits of injecting cold fluid into the descending part of the convection loop. This conclusion, however, came from the analysis of a small set of the production cases with only one flow rate of 0.2 kg/s. Further investigation now examines how the choice of the particular production arrangement influences energy recovery at higher geofluid flow rates.

The three line plots in Fiures 6.2, 6.3 and 6.4 show that the statement about advantages of the regular design holds true for small and medium production flow rates. Once the geofluid flow rate becomes high (such as 20 kg/s), forced convection overshadows all effects of natural convection and dip.

The Figure 6.4 is particularly interesting in this sense, small thickness cases with dips of 0, 2, and 15 degrees after 30 years recover much more energy with displacement than with regular design. Thicker and low permeability systems, however, still exhibit advantages in the regular design. That is, the same system can produce differently depending on anticipated

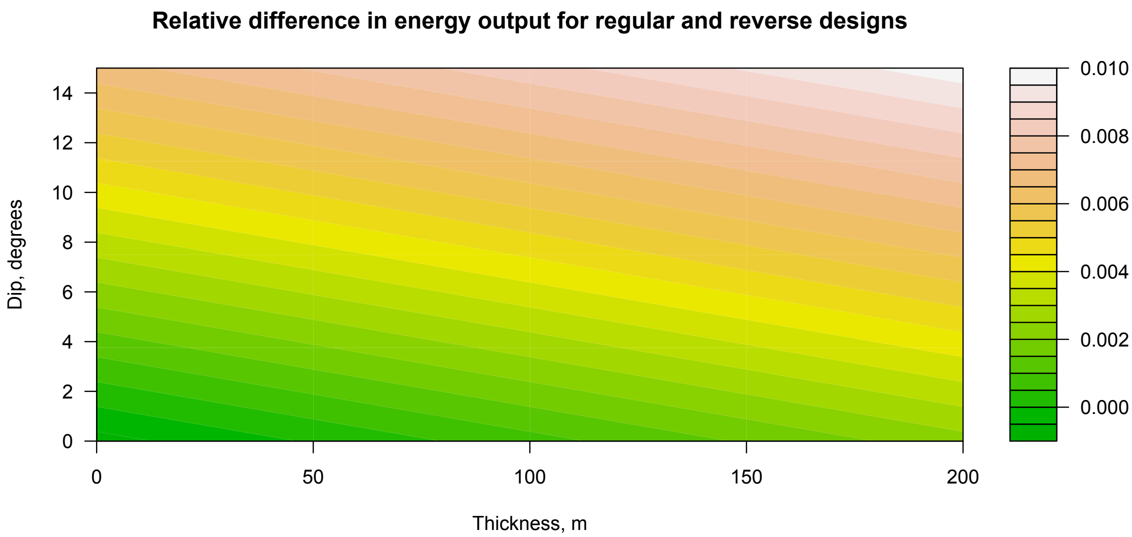

Figure 6.1: Contour plot of relative increase in energy recovery for regular production design compared to reverse one for the cases produced at 0.2 kg/s for 10 years. Notice the effect of increasing dip and thickness on relative increase in recovery. The contoured variable is $2(E_{\text{reg}} - E_{\text{rev}})/(E_{\text{reg}} + E_{\text{rev}})$

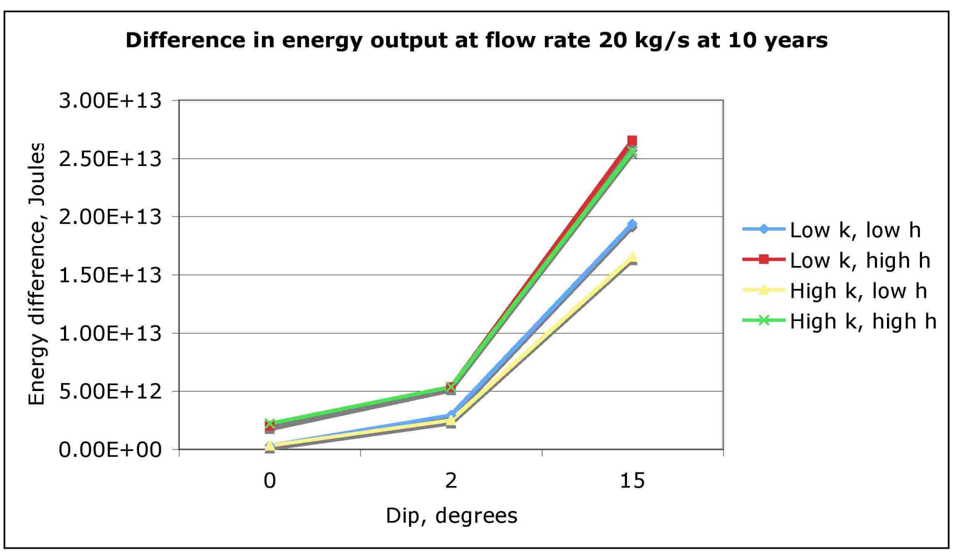

Figure 6.2: Line plot for production cases initialized with natural convection and produced at 20 kg/s flow rate per 100 m of wellbore at 10 years. Difference in energy output for regular and reverse production design is plotted for varying dip. Regular design shows better performance than reverse one for all cases.

duration and scale (high or low flow rate) of heat extraction as well as well placement. Thus, the most significant geometric and petrophysical factors should be considered in connection

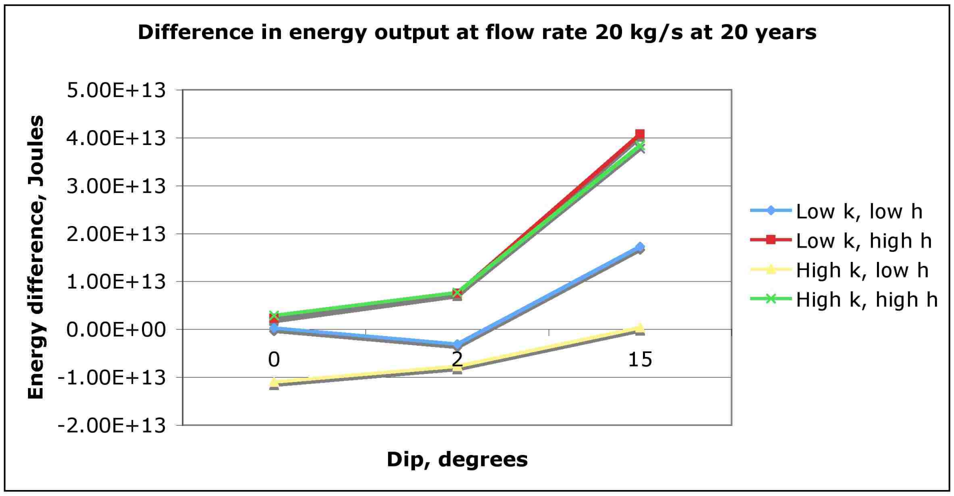

Figure 6.3: Line plot for production cases initialized with natural convection and produced at 20 kg/s flow rate per 100 m of wellbore at 20 years. Difference in energy output for regular and reverse production design is plotted for varying dip. Regular design outperforms reverse one in thick systems only.

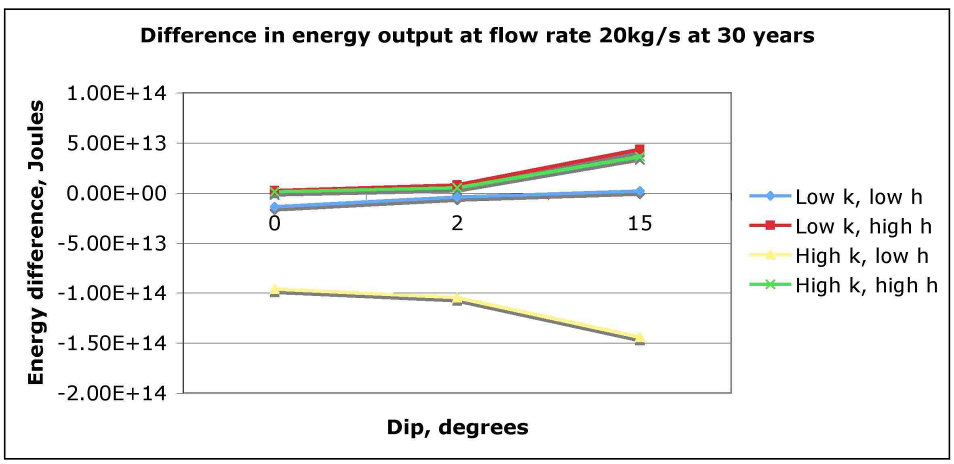

Figure 6.4: Line plot for production cases initialized with natural convection and produced at 20 kg/s flow rate per 100 m of wellbore at 30 years. Difference in energy output for regular and reverse production design is plotted for varying dip. Reverse design produces more energy than regular one in thin systems and comparable amounts of energy in thick systems.

to production arrangement if the goal is to increase thermal energy recovery from the system of interest.

6.2 Natural Convection Initialization: Further Ideas

Another phenomenon that might affect energy output is initialization with natural convection. Similarly to the production design analysis, a subset of cases initialized without and with natural convection (no CO_2 were included) was used to obtain a column of differences of energy outputs. Before the analysis, the expectation was that flat systems would not be significantly affected by initilization. Inclined cases, however, should exhibit an increasing difference in energy output. This occurs due to natural convection initialization that ensures a wider temperature spectrum (as it was discussed in Chapter 3) and, thus, a higher enthalpy of the produced geofluid. The contour plot in Fig. 6.5 corroborates the expectation based on theory and previous experimental research. Indeed, energy recovery from the systems with zero or nearly zero dips are virtually not affected by the initialization. Meanwhile, the upper portion of the contour plot corresponding to high dips shows relative differences in outputs from convection and no convection cases $(2(E_{\text{conv}} - E_{\text{no}})/(E_{\text{conv}} + E_{\text{no}}))$ of five percent; convection cases always recover more heat.

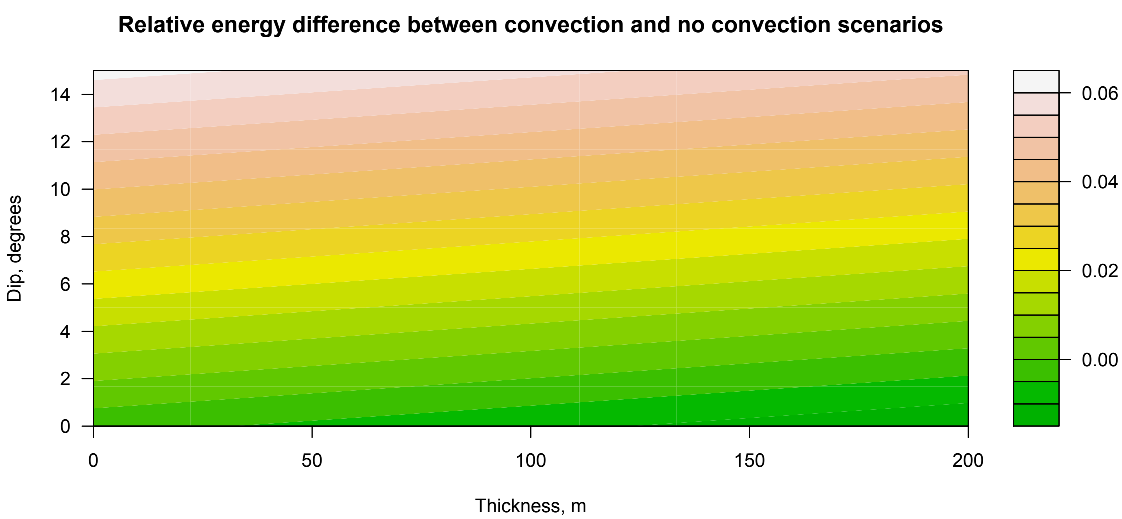

Figure 6.5: Contour plot of relative increase in energy recovery for the cases initialized without natural convection compared to the cases with natural convection, $2(E_{\text{conv}} - E_{\text{no}})/(E_{\text{conv}} + E_{\text{no}})$. The systems are produced at 0.2 kg/s for 10 years. The systems with convection included always have a higher heat recovery. Dip has a greater impact on relative increase in recovery than thickness of a system.

Natural convection modeling in this thesis (chapter 3) emphasizes the importance of bounding layers and the quiescent period. Although the top and bottom bounding layers have the greatest effect on temperature profile in a quiescent system (due to the areal extent of these layers), it would be interesting to investigate the impact of side bounding layers. One potential benefit of modeling a side bounding is ability to incorporate a salt dome with its heat fluxes into the geomodel. Introduction of additional bounding layers (or heat sources) will impact the duration of the quiescent period; therefore, a more thorough analysis with an experimental design might be necessary to establish the time span after which convection becomes constant.

Another factor that affects natural convection and its stabilization is geofluid salinity. Salinity effects were intentionally omitted in this study to focus on geometry and petrophysical properties of the geothermal systems, but future research should examine salinity. Investigation of double-diffusion and salt fingering in oceanography reveals implications of thermo-haline convection on energy transfer which should not be disregarded for fluid saturated geopressured systems (Schmitt 1994). Study of nonuniform salinity and its impact on convection patterns in quiescent geopressured systems prior to heat extraction is another area that could improve our production planning.

6.3 CO_2 Sequestration in Geopressured Aquifers

In addition to natural convection initialization and production design, it is important to establish whether strategic placement of a horizontal CO_2 injection well has a positive impact on energy recovery. This analysis uses a subset of cases with natural convection initialization, because no simulations with CO_2 injection and without natural convection were run. Based on previous theoretical and experimental research about CO_2 sequestration and the fact that the supercritical gas injector is spatially isolated from the heat extraction well, we expect comparable or better thermal energy recovery from the cases with simultaneous CO_2 injection. Figure 6.6 substantiates this expectation and demonstrates that differences in energy outputs, $2(E_{\mathrm{CO2}} - E_{\mathrm{conv}})/(E_{\mathrm{CO2}} + E_{\mathrm{conv}})$, are nonnegative, indicating better performance of the cases with CO_2 injection. Again, dip aids higher energy recovery.

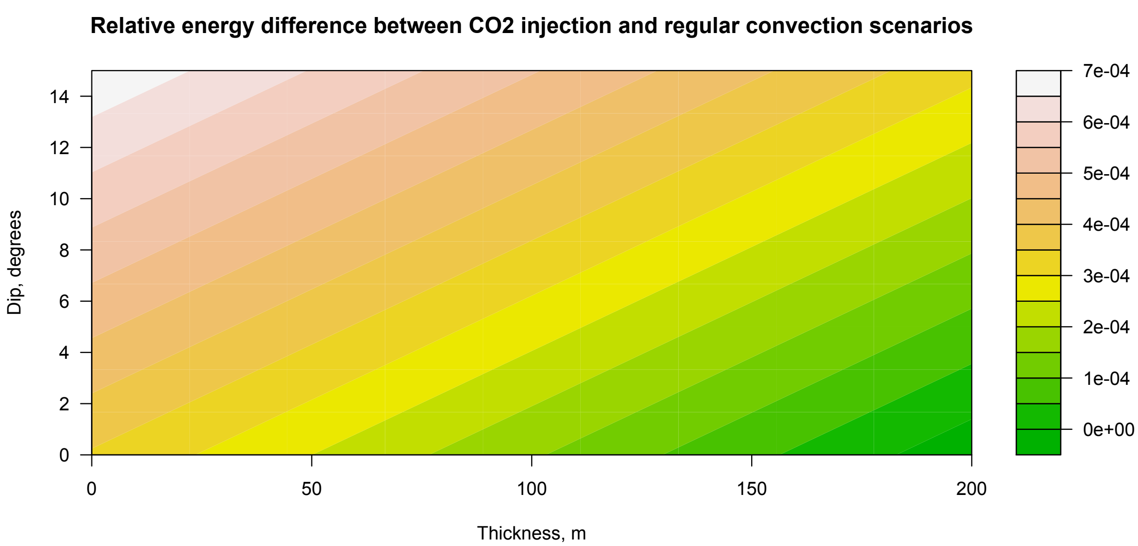

Figure 6.6: Contour plot of relative increase in energy recovery for the cases with CO_2 injection compared to regular production. The systems are produced at 0.2 kg/s for 10 years. CO_2 injection rate is 0.0001 kg/s. Both dip and thickness influence the recovery.

Can CO_2 sequestration be done simultaneously with heat extraction, without impairing heat recovery? The simulations (Fig. 6.6) show that injection of small amounts of supercritical CO_2 away from the geofluid producer and injector is beneficial. Because forced convection is the dominant component of coupled convection, it is logical to conclude that increased energy output in the cases with CO_2 injection is due to enhanced displacement rather than gas dissolution and subsequent density density–driven convection. This conclusion, nevertheless, should not undermine further attempts to simultaneously harvest geothermal heat and sequiester carbon dioxide, if CO_2 injection rate is above chosen 0.0001 kg/s per 100 m. The sequestration rate could be increased to match those in major CO_2 sequestration projects (NETL 2008). The choice of the rate of 0.0001 kg/s was dictated by the necessity to compare against the same production arrangement in different geologic systems (10 fold difference in permeability, high and zero dip reservoirs) and does not mean that this rate (0.0001 kg/s per 100 m) is an upper limit for each sedimentary geothermal aquifer. For 1000 mD and 200 m thick systems the CO_2 injection rate could have been much higher than 0.0001 kg/s, but would cause serious simulation problems due to rapid pressure buildup in lower permeability reservoirs. Therefore, the next step in research is to demonstrate whether aquifers with thermodynamic and petrophysical properties favorable for CO_2 sequestration can also be prolific geothermal systems. One possibility would be to produce a limited amount of geofluid to lower the injection pressure (section 6.4, later).

Geothermal development during CO_2 sequestration might be particularly appealing when there is a concern about seal integrity. Recent research suggests that placing a horizontal water injector above a CO_2 injector can prevent the plume with high concentration of the supercritical gas from rising to the top of the reservoir and creating a potentially dangerous scenario with leakage to the surface (Anchliya 2009). Simulations run for this study also showed that such dynamic control over the CO_2 plume can be attained (Figs. 6.7 and 6.8) and CO_2 concentration can be significantly reduced.

In Figure 6.7 mass fraction of liquid CO_2 rises above 0.02 and the plume has a well-defined shape that will slowly flow to the top of the reservoir and accumulated under the caprock. The Figure 6.8 with an additional water injection well shows a completely different picture after 30 years of sequestration. The maximum CO_2 concentration is ten times lower that in previous case and the plume is poorly defined and driven downdip. These qualitative results look promising in attempt to gain dynamic control over CO_2 plume in sequestration projects and to preserve caprock integrity.s

6.4 Initial Depletion Production for Undisturbed Geopressured Aquifers

For the purposes of having three suites of simulations with comparable initial thermodynamic properties (temperature and pressure), pressure was intentionally lowered below geopressure. Otherwise, injection of CO_2 and modeling high dip systems would not be possible with the software tool chosen. This lowering of pressure must be considered when assessing productivity, heat content, and CO_2 sequestration. If the initial pressure is brought back to about 80 MPa (as it was calculated for Camerina A sand), it will have an impact on enthalpy of the produced geofluid and the possibility of reinjection into the same formation. In other words, for a geopressured aquifer found at a depth similar to that of Camerina A sand, an

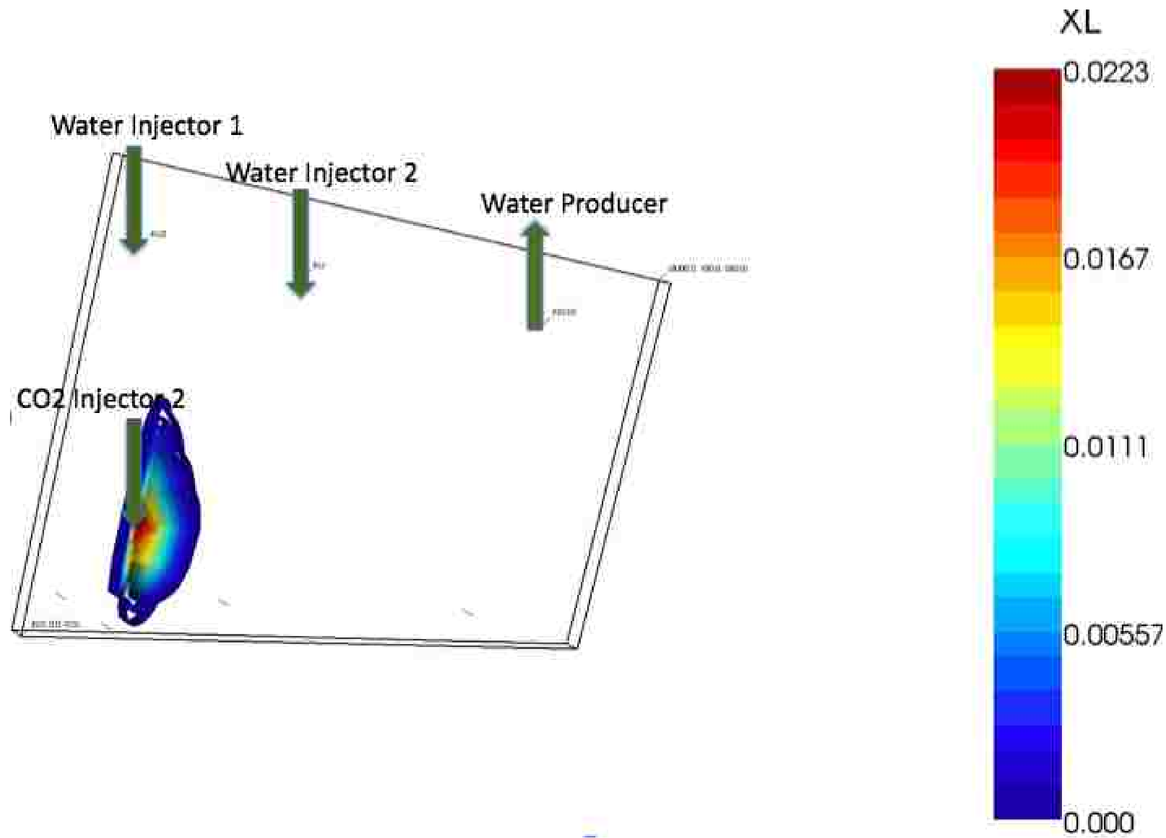

Figure 6.7: CO_2 injection with heat extraction and no water injection in well 1. Snapshot of liquid CO_2 mass fraction is taken after 30 years of injection. The supercritical gas mixes with geolfuid slowly creating a well-defined plume of high concentration that will present danger to the caprock in future. The reservoir is a 2D geomodel with length of 4000 m, width of 100 m, and height of 200 m (with 10-fold exaggeration in z-direction). Permeability is 1 D and porosity is 0.2. Gas injection rate is 0.003 kg/s. The plot's legend represents mass fraction of liquid CO_2 (no gas phase).

initial period of depletion will be required before cooled geofluid can be reinjected and CO_2 sequestration devised. The degree of depletion would have to be engineered to ensure that surface subsidence was neglibible or within acceptable limits.

6.5 Wellbore Cooling for Fractured Systems

Chapter 3 discussed the possibility of heat extraction by means of wellbore cooling without withdrawal of geofluid from the subsurface. Though an attractive concept, the analysis showed that permeability of a reservoir suitable for development with such production technique should be very high (up to a thousand darcies). Sedimentary aquifers with high formation temperatures and such high permeabilities are extremely rare. Only hydrothermal systems with existing or artificially created fracture patterns have all the properties that might make wellbore cooling feasible.

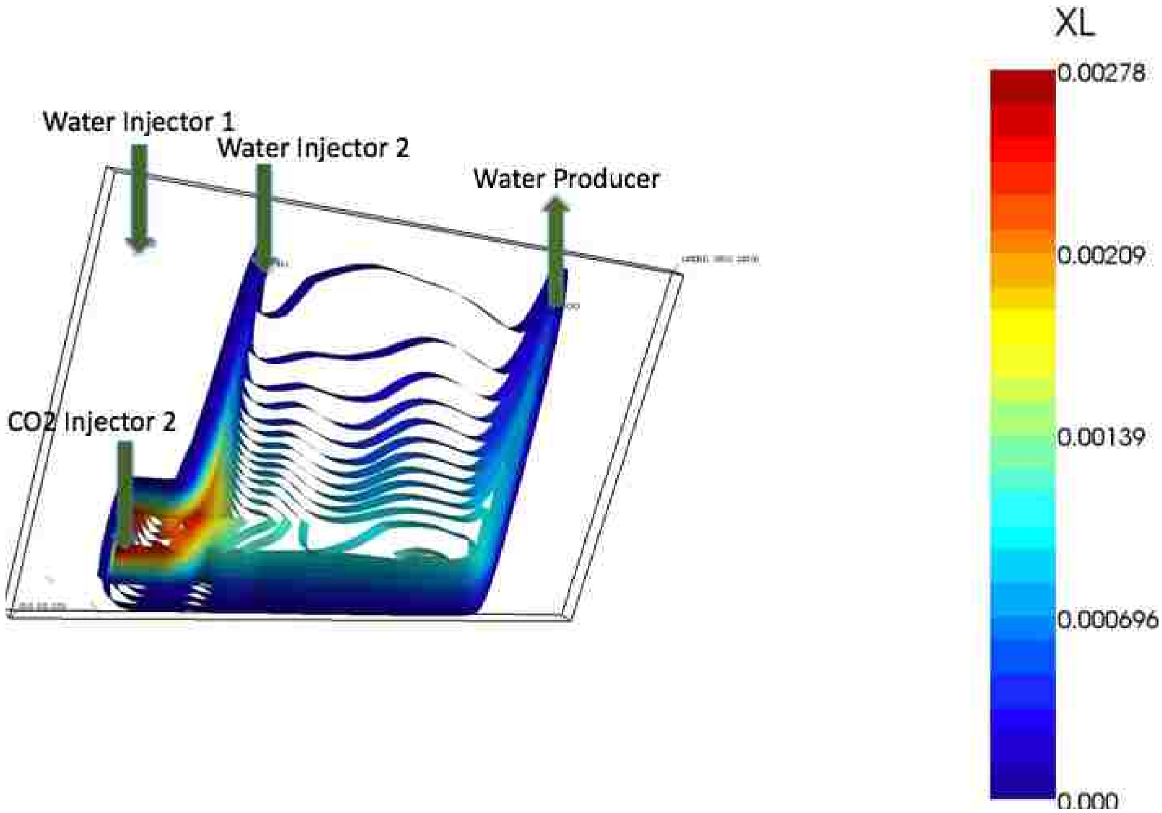

Figure 6.8: CO_2 injection with heat extraction and an additional dynamic control well 1. Snapshot of liquid CO_2 mass fraction is taken after 30 years of injection. The supercritical gas mixes with geolfuid faster. This leads to lower gas concentration and prevents formation of the plume. The reservoir is a 2D geomodel with length of 4000 m, width of 100 m, and height of 200 m (with 10-fold exaggeration in z-direction). Permeability is 1 D and porosity is 0.2. Gas injection rate is 0.003 kg/s. The plot's legend represents mass fraction of liquid CO_2 (no gas phase).

Hydrothermal reservoirs are not typical for the Gulf coast environment and this is why they are not modeled in this thesis. Examining wellbore cooling in a hydrothermal system would require a different conceptual model, because performance of such reservoirs depends on proper characterization of its fracture pattern. Though a challenging problem in itself, wellbore cooling may provide a new economic heat extraction methods for high-enthalpy systems.

6.6 Monobore Production Strategy

Instead of using a convectional arrangement of injectors and producers with surface facilities for energy conversion, one might envision a monobore design (Fig. 6.9). The monobore contains a downhole heat exchanger that cools the geofluid inside the wellbore and reinjects it back into the formation without lifting the water to the surface. Only the secondary fluid (probably an organic working fluid with a low boiling point) is circulated to the surface turbine and condeser, circulating in a closed loop. The monobore design has a number of advantages over the standard geothermal production setup. First, it requires fewer wells, though the configuration of them could be quite complex. Second, the surface footprint is minimal, because the downhole heat exchanger eliminated the problem of surface handling of the geofluid. Third, rock compaction might be reduced due to relatively close reinjection. This is an appealing production approach that will require a more detailed investigation for commercial feasibility.

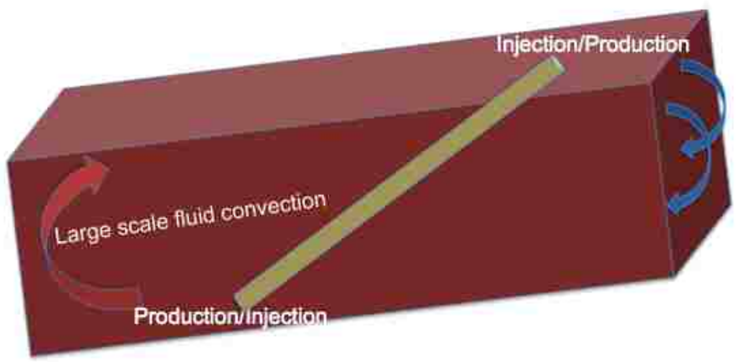

Figure 6.9: Conceptual design for monobore production. The monobore is an inclined wellbore with production/injection segments near the top/bottom of the reservoir. The choice of optimal placement of production/injection segments requires addition investigation.

Chapter 7

Conclusions

This thesis investigated the effects of coupled convection and CO_2 injection for heat extraction from sedimentary geothermal aquifers. The analysis showed that there are benefits in characterizing natural convection pattern prior to geofluid production, because it provides means for comparison between alternative designs. Statistical examination of the simulation results confirmed the expectation that dip controls the intensity of natural convection and aids forced convection at moderate production rates. Juxtaposition of simulation suites with and without CO_2 injection revealed that the greenhouse gas injection had a positive impact on thermal energy recovery.

7.1 Recommendations for Further Research

This research opened up some interesting venues for future research.

- CO_2 sequestration at higher gas injection rates with simultaneous heat harvesting and dynamic control over the gas plume might increase revenue. Because both carbon dioxide sequestration and saline aquifer geothermal development are marginally profitable, this approach might make the combination project more economically attractive.

- The monobore production design has a potential of decreasing surface footprints and testing new well design ideas. Economic and engineering feasibility of downhole heat exchangers for deep geothermal development is yet to be demonstrated.

- A comparative study of TOUGH2 and alternative software tools might provide calibration of the obtained results and resolution for problems involving heat fluxes. In this thesis the analysis of heat fluxes to the wellbore region or in and out of the reservoir were used sparingly and qualitatively. The reason for this is limitations imposed by output from TOUGH2 software that does not separate conduction, convection, and radiation. It would be particularly helpful to have such capability for wellbore cooling modeling and for evaluation of heat fluxes from bounding layers.

- One can envision an investigation of effects of nonuniform salinity and heat sources due salt domes on natural convection pattern. Thermohaline convection is an important factor in heat transfer in the Gulf coast environment that might have an impact on geothermal heat extraction.

- Wellbore cooling design for enhanced geothermal (or fractured) systems requires further numerical study and, in case of success, field application.

Bibliography

Anchliya, A. 2009. "Aquifer Management for CO2 Sequestration." Master's thesis, Texas A and M University.

Battistell, A., C. Calore, and K. Pruess. 2007. "The Simulator TOUGH2/EWASG for Modeling Geothermal Reservoirs with Brines and Non-Condensible Gas." *Geothermics* 26 (4): 437–464.

Curtice, R. J., and E. D. Dalrymple. 2004. "Just the cost of doing business." *World Oil*, pp. 77–78.

Dullien, F. A. 1979. *Porous Media: Fluid Transport and Pore Structure.* Academic Press.

Ewing, T. E, P. R Light, and N. Tyler. 1984. "Thermal and Diageneic History of the Pleasant Bayou - Chocolate Bayou Area, Brazoria County, Texas." 34:341–348.

Farajzadeh, R. et al. 2007. "Numerical Simulation of Density-Driven Natural Convection in Porous Media with Application for CO_2 Injection Projects." *International Journal of Heat and Mass Transfer* 50:5054–5064.

Garcia, J. 2001. "Density of Aqueous Solution of CO_2." Technical Report LBNL-49023, Lawrence Berkeley National Laboratory.

Grant, M. 1982. *Geothermal Reservoir Engineering.* New York: Academic Press Inc.

Gray, T. A. 2010, August. "Geothermal Resource Assessment of the Guyedan Salt Dome and the Adjacent Southeast Guyedan Field, Vermilion Parish, Louisiana." pp. 4, 20-40, Louisiana State University.

Griggs, J. 2004, August. "A Re-Evaluation of Geopressured Geothermal Aquifers as an Energy Resource." Master's thesis, Louisiana State University.

Hanor, J. 1987. "Kilometre-scale thermohaline overturn of pore fluid in the Louisiana Gulf

Coast." *Nature* 327:502–503.

Horne, R. 1975. "Transient Effects in Geothermal Convective Systems." Ph.D. diss., Department of Theoretical and Applied Mechanics, Auckland, New Zealand.

Kneafsey, T., and K. Pruess. 2009. "Laboratory Flow Experiments for Visualizing Carbon-Dioxide-Induced, Density-Driven Brine Convection." *Transport in Porous Media*.

MIT. 2006. "The Future of Geothermal Energy: Impact of Enhanced Geothermal Systems (EGS) on the United States in the 21st Century." Technical Report, Renewable Energy and Power Department, Idaho National Laboratory.

NETL. 2008. "Carbon Sequestration Atlas of the United States and Canada." Technical Report, U.S. Department of Energy.

Nield, D., and A. Bejan. 2006. *Convection in Porous Media. Third Edition.* New York: Springer Science+Business Media, Inc.

Panda, M. N., and L. W. Lake. 1994. "Estimation of Single-Phase Permeability from Parameters of Particle-Size Distribution." *AAPG Bulletin* 78 (7): 1019–1028.

Pruess, K., C. Oldenburg, , and G. Moridis. 1999. "TOUGH2 User's Guide, Version 2.0." Technical Report LBNL-43134, Lawrence Berkeley National Laboratory.

Riney, T. D. 1992. "Pleasant Bayou Geopressured-Geothermal Reservoir Analysis - Octpber 1991." *Journal of Energy Resources Technology* 114 (December): 314–322.

Schmitt, R. 1994. "Double Diffusion in Oceanography." *Annual Review FLuid Mechanics* 26:255–85.

Schubert, G., and J. Straus. 1978. "Three-Dimensional and Multicellular Steady and Unsteady Convection in Fluid-Saturated Porous Media at High Rayleigh Numbers." *United States Government Printing Office, Washington.*

Sorey, M. 1979. "Numerical Modeling of Liquid Geothermal Systems." *Journal of Fluid Mechanics* 94 (1): 25–38.

Szalkowski, S., and J. Hanor. 2003. "Spatial Variations in the Salinity of Produced Waters from Southwestern Louisiana." *GCAGS/GCSSEPM Transactions* 53:798–806.

Team, R Development Core. 2008. *R: A Language and Environment for Statistical Computing.* Vienna, Austria: R Foundation for Statistical Computing.

White, D. F., and D. L. Williams. 1975. "Assessment of Geothermal Resource of the United States." Technical Report, U.S. Geological Survey (USGS) Circular 726.

Appendix A

Nomenclature

Table A.1: Nomenclature of Symbols

Symbol	Name	Units
α	chemical component	–
β	phase	aqueous, gaseous, solid
γ	thermal expansivity of fluid	
Γ	surface of control volume	m^2
Δ	change in	units of variable
κ	conductivity of rock matrix	W/m ℃
μ	viscosity	Pa-s
π		=3.14
ρ	density	kg/m^3
ϕ	porosity	fraction or percent
c	fluid specific heat	J/kg ℃
d	dimension of square cross-section	m
g	gravity acceleration	$=9.81 m/s^2$
k	permeability	m^2
t	time	s
T	temperature	℃
W	power output	kW
q	flow rate	kg/s

Table A.1: List of symbols

Appendix B

Experimental Design

Table B.1: Factorial Experimental Design

Design Number/Parameter	Permeability	Thickness	Dip
1	100 md	100 m	0 deg
2	100 md	100 m	2 deg
3	100 md	100 m	15 deg
4	100 md	200 m	0 deg
5	100 md	200 m	2 deg
6	100 md	200 m	15 deg
7	1000 md	100 m	0 deg
8	1000 md	100 m	2 deg
9	1000 md	100 m	15 deg
10	1000 md	200 m	0 deg
11	1000 md	200 m	2 deg
12	1000 md	200 m	15 deg

Appendix C

TOUGH2 Input Decks

Typical TOUGH2 input file specifying rock properties (ROCKS), equation of state (MULTI), computation parameters (PARAM), solver of the systems of equations (SOLVR), times for desired output (TIMES) and grid blocks with their geometric and initial thermodynamic properties (ELEME). The following sample of TOUGH2 input file provides the header and the truncated ELEME part for brevity.

```
TOUGH2 Analysis
ROCKS----1----*----2----*----3----*----4----*----5----*----6----*----7----*----8
ROCK1    3    2600.0    0.2000001.000e-0131.000e-0131.000e-013       2.0    1000.0
2.000e-008       0.0       2.0       0.0       0.0
    1      0.200000  0.100000  0.900000  0.700000
    8
ROCK2    3    2600.0       0.0       0.0       0.0       0.0       2.01.000e+021
      0.0       0.0       2.0       0.0       0.0
    1      0.200000  0.100000  0.900000  0.700000
    8

MULTI----1----*----2----*----3----*----4----*----5----*----6----*----7----*----8
    1    2    2    6
START----1----*----2----*----3----*----4----*----5----*----6----*----7----*----8
PARAM----1-MOP* 123456789012345678901234----*----5----*----6----*----7----*----8
 8 2 200      1000000000 0001  03 000   0
      0.03.154e+010     100.0       0.0            9.8100       4.0       1.0
1.000e-005       1.0                 1.0       1.0

SOLVR----1----*----2----*----3----*----4----*----5----*----6----*----7----*----8
3  Z1   O0  0.1000001.000e-006
TIMES----1----*----2----*----3----*----4----*----5----*----6----*----7----*----8
   31   31
      1.03.150e+0076.310e+0079.460e+0071.260e+0081.580e+0081.890e+0082.210e+008
2.520e+0082.840e+0083.150e+0083.470e+0083.780e+0084.100e+0084.420e+0084.730e+008
5.050e+0085.360e+0085.680e+0085.990e+0086.310e+0086.620e+0086.940e+0087.250e+008
7.570e+0087.880e+0088.200e+0088.510e+0088.830e+0089.150e+0089.460e+008
ELEME----1----*----2----*----3----*----4----*----5----*----6----*----7----*----8
  2 1          ROCK1  40000.0       0.0       1.0      10.0      50.0      30.0
  2 2          ROCK1  40000.0       0.0       1.0      30.0      50.0      30.0
  2 3          ROCK1  40000.0       0.0       1.0      50.0      50.0      30.0
  2 4          ROCK1  40000.0       0.0       1.0      70.0      50.0      30.0
  2 5          ROCK1  40000.0       0.0       1.0      90.0      50.0      30.0
  2 6          ROCK1  40000.0       0.0       1.0     110.0      50.0      30.0
  2 7          ROCK1  40000.0       0.0       1.0     130.0      50.0      30.0
  2 8          ROCK1  40000.0       0.0       1.0     150.0      50.0      30.0
  2 9          ROCK1  40000.0       0.0       1.0     170.0      50.0      30.0
  210          ROCK1  40000.0       0.0       1.0     190.0      50.0      30.0
  211          ROCK1  40000.0       0.0       1.0     210.0      50.0      30.0
  ...
```

Appendix D

Results and Illustrations

D.1 Natural Convection Modeling

Table D.1: 2D TOUGH2 runs for quiescent systems with varying dip

	length (m)	dip (deg)	h (m)	Ra	Ra critical
1	2000	0	30	0.26	39.43
2	2000	1	30	0.61	0.68
3	2000	2	30	1.84	1.37
4	2000	4	30	6.19	2.75
5	2000	8	30	22.29	5.48
6	2000	16	30	82.61	10.86
7	2000	32	30	296.07	20.88

Table D.2: 2D TOUGH2 runs for quiescent systems with varying thickness

	length (m)	dip (deg)	h (m)	Ra	Ra critical
1	4000	4	10	20.82	2.75
2	4000	4	30	22.42	2.75
3	4000	4	90	27.19	2.75
4	4000	4	270	41.41	2.75

Table D.3: 2D TOUGH2 runs for quiescent systems with varying length

	length (m)	dip (deg)	h (m)	Ra	Ra critical
1	1000	4	30	01.84	2.75
2	2000	4	30	6.19	2.75
3	4000	4	30	22.42	2.75
4	8000	4	30	85.29	2.75
5	16000	4	30	329.32	2.75

Table D.4: 2D TOUGH2 runs for quiescent systems with varying permeability

	permeability (m^2)	length (m)	dip (deg)	h (m)	Ra	Ra critical
1	1E-13	4000	4	10	7.46	2.75
2	3E-13	4000	4	30	22.38	2.75
3	9E-13	4000	4	90	67.15	2.75

Table D.5: 2D TOUGH2 runs for determining an average porosity value

	porosity	initial energy (J)	remaining energy (J)	extracted energy (J)
1	0.05	3.6E+15	2.7E+15	9E+14
2	0.1	3.7E+15	2.8E+15	9E+14
3	0.15	3.8E+15	2.9E+15	8.9E+14
4	0.2	3.9E+15	3E+15	8.8E+14
5	0.25	4E+15	3.1E+15	8.8E+14
6	0.3	4E+15	3.2E+15	8.7E+14

Table D.6: Rayleigh number and its critical values for production cases from the experimental design

Case	Rayleigh number	Critical Rayleigh number
1 (100 md, 100m, 0 deg)	0.956	39.478
2 (100 md, 100m, 2 deg)	2.669	1.377
3 (100 md, 100m, 15 deg)	103.956	10.217
4 (100 md, 200m, 0 deg)	3.827	39.478
5 (100 md, 200m, 2 deg)	4.004	1.377
6 (100 md, 200m, 15 deg)	1108.907	10.217
7 (1000 md, 100m, 0 deg)	9.568	39.478
8 (1000 md, 100m, 2 deg)	26.699	1.377
9 (1000 md, 100m, 15 deg)	1039.566	10.217
10 (1000 md, 200m, 0 deg)	38.272	39.478
11 (1000 md, 200m, 2 deg)	40.049	1.377
12 (1000 md, 200m, 15 deg)	1089.070	10.217

D.2 Cumulative Energy Calculation

Energy calculation for Case 1 regular design with a production flow rate of 0.2 kg/s per 100 m of wellbore.

Time, s	Enthalpy, J/kg	Energy, J	Cum Energy, J
0	589150	0	0
1	589050	117820	117820
3.15E+07	588990	3.71E+12	3.71E+12
6.31E+07	588940	3.72E+12	7.43E+12
9.46E+07	588900	3.71E+12	1.11E+13
1.26E+08	588870	3.70E+12	1.48E+13
1.58E+08	588830	3.77E+12	1.86E+13
1.89E+08	588810	3.65E+12	2.23E+13
2.21E+08	588780	3.77E+12	2.60E+13
2.52E+08	588750	3.65E+12	2.97E+13
2.84E+08	588730	3.77E+12	3.34E+13
3.15E+08	588710	3.65E+12	3.71E+13
3.47E+08	588690	3.77E+12	4.09E+13
3.78E+08	588670	3.65E+12	4.45E+13
4.10E+08	588650	3.77E+12	4.83E+13
4.42E+08	588640	3.77E+12	5.20E+13
4.73E+08	588620	3.65E+12	5.57E+13
5.05E+08	588610	3.77E+12	5.95E+13
5.36E+08	588590	3.65E+12	6.31E+13
5.68E+08	588580	3.77E+12	6.69E+13
5.99E+08	588560	3.65E+12	7.05E+13
6.31E+08	588550	3.77E+12	7.43E+13
6.62E+08	588540	3.65E+12	7.79E+13
6.94E+08	588530	3.77E+12	8.17E+13
7.25E+08	588520	3.65E+12	8.54E+13
7.57E+08	588510	3.77E+12	8.91E+13
7.88E+08	588500	3.65E+12	9.28E+13
8.20E+08	588490	3.77E+12	9.65E+13
8.51E+08	588480	3.65E+12	1.00E+14
8.83E+08	588470	3.77E+12	1.04E+14
9.15E+08	588460	3.77E+12	1.08E+14
9.46E+08	588460	3.65E+12	1.11E+14

D.3 Result Table for Production Cases

Table D.7: Energy output after 10 years of production at 0.2 kg/s geofluid flow rate without and with convection as well as CO_2 injection

	case	perm (md)	h (m)	dip (deg)	co2 (kg/s)	design (1,0)	convec (1,0)	energy (J)
1	1	100	100	0	0	1	1	3.7E+13
2	2	100	100	2	0	1	1	3.8E+13
3	3	100	100	15	0	1	1	4.1E+13
4	4	100	200	0	0	1	1	3.7E+13
5	5	100	200	2	0	1	1	3.8E+13
6	6	100	200	15	0	1	1	4.1E+13
7	7	1000	100	0	0	1	1	3.7E+13
8	8	1000	100	2	0	1	1	3.8E+13
9	9	1000	100	15	0	1	1	4.1E+13
10	10	1000	200	0	0	1	1	3.7E+13
11	11	1000	200	2	0	1	1	3.8E+13
12	12	1000	200	15	0	1	1	4.1E+13
13	1	100	100	0	0	0	1	3.7E+13
14	2	100	100	2	0	0	1	3.7E+13
15	3	100	100	15	0	0	1	3.8E+13
16	4	100	200	0	0	0	1	3.6E+13
17	5	100	200	2	0	0	1	3.6E+13
18	6	100	200	15	0	0	1	3.8E+13
19	7	1000	100	0	0	0	1	3.7E+13

continued on next page

continued from previous page								
	case	perm (md)	h (m)	dip (deg)	co2 (kg/s)	design (1,0)	convec (1,0)	energy (J)
20	8	1000	100	2	0	0	1	3.7E+13
21	9	1000	100	15	0	0	1	3.8E+13
22	10	1000	200	0	0	0	1	3.6E+13
23	11	1000	200	2	0	0	1	3.6E+13
24	12	1000	200	15	0	0	1	3.8E+13
25	1	100	100	0	0	1	0	3.7E+13
26	2	100	100	2	0	1	0	3.7E+13
27	3	100	100	15	0	1	0	3.7E+13
28	4	100	200	0	0	1	0	3.7E+13
29	5	100	200	2	0	1	0	3.7E+13
30	6	100	200	15	0	1	0	3.7E+13
31	7	1000	100	0	0	1	0	3.7E+13
32	8	1000	100	2	0	1	0	3.7E+13
33	9	1000	100	15	0	1	0	3.7E+13
34	10	1000	200	0	0	1	0	3.7E+13
35	11	1000	200	2	0	1	0	3.7E+13
36	12	1000	200	15	0	1	0	3.7E+13
37	1	100	100	0	0	0	0	3.7E+13
38	2	100	100	2	0	0	0	3.7E+13
39	3	100	100	15	0	0	0	3.7E+13
40	4	100	200	0	0	0	0	3.7E+13
41	5	100	200	2	0	0	0	3.7E+13
42	6	100	200	15	0	0	0	3.7E+13
43	7	1000	100	0	0	0	0	3.7E+13
44	8	1000	100	2	0	0	0	3.7E+13
45	9	1000	100	15	0	0	0	3.7E+13
46	10	1000	200	0	0	0	0	3.7E+13
47	11	1000	200	2	0	0	0	3.7E+13
48	12	1000	200	15	0	0	0	3.7E+13
49	1	100	100	0	0.0001	1	1	3.7E+13
50	2	100	100	2	0.0001	1	1	3.8E+13
51	3	100	100	15	0.0001	1	1	4.1E+13
52	4	100	200	0	0.0001	1	1	3.7E+13
53	5	100	200	2	0.0001	1	1	3.8E+13
54	6	100	200	15	0.0001	1	1	4.1E+13
55	7	1000	100	0	0.0001	1	1	3.7E+13
56	8	1000	100	2	0.0001	1	1	3.8E+13
57	9	1000	100	15	0.0001	1	1	4.1E+13
58	10	1000	200	0	0.0001	1	1	3.7E+13
59	11	1000	200	2	0.0001	1	1	3.8E+13
60	12	1000	200	15	0.0001	1	1	4.1E+13
61	1	100	100	0	0.0001	0	1	3.7E+13
62	2	100	100	2	0.0001	0	1	3.7E+13
63	3	100	100	15	0.0001	0	1	3.8E+13
64	4	100	200	0	0.0001	0	1	3.6E+13
65	5	100	200	2	0.0001	0	1	3.6E+13
66	6	100	200	15	0.0001	0	1	3.8E+13
67	7	1000	100	0	0.0001	0	1	3.7E+13
68	8	1000	100	2	0.0001	0	1	3.7E+13
69	9	1000	100	15	0.0001	0	1	3.8E+13
70	10	1000	200	0	0.0001	0	1	3.6E+13
71	11	1000	200	2	0.0001	0	1	3.6E+13
72	12	1000	200	15	0.0001	0	1	3.8E+13

D.4 Model Fitting

R script and output for the model calculated by the stepwise regression procedure.

```
> fit.energy.final <- lm(energy ~ dip + convec+dip:convec,data=ener)
> anova(fit.energy.final)
Analysis of Variance Table

Response: energy
           Df     Sum Sq    Mean Sq F value    Pr(>F)    
dip         1 3.9343e+25 3.9343e+25 56.2609 1.766e-10 ***
convec      1 4.3403e+24 4.3403e+24  6.2066   0.01517 *  
dip:convec  1 1.9917e+25 1.9917e+25 28.4812 1.174e-06 ***
Residuals  68 4.7552e+25 6.9930e+23                      
---
Signif. codes:  0 '***' 0.001 '**' 0.01 '*' 0.05 '.' 0.1 ' ' 1
```

D.5 Contour Plot for Difference of Energy Output for Cases Initialized without and with Natural Convection.

R script and output for difference in energy output for cases initialized without and with natural convection. The subset used for this analysis is comprised of cases produced at 0.2 kg/s geofluid flow rate after 10 years of production. No cases with CO_2 injection are included.

```
ener <- read.csv("diffnoconvandconv.csv")

# define a new model
fit.energy.final <- lm(den ~ dip +perm ,data=ener)

# make grid with h and dip
dip <- seq(0,15,length.out=100)
perm <- seq(100,1000,length.out=10)
g.perm.dip <- expand.grid(perm=perm,dip=dip)

# predict value of energy output based on the model
g.perm.dip <-
data.frame(g.perm.dip,ener.model=predict(fit.energy.final,g.perm.dip
))

# contour plot the result
plot.var = matrix(g.perm.dip$ener.model, nrow=10)
filled.contour(perm, dip, plot.var,
color=terrain.colors,xlab="Permeability, md",ylab="Dip, degrees",
main="Energy difference between no convection and convection
scenarios (J)")
```

Appendix E

Supplementary Scripts and R Code

E.1 Awk Initialization Script

Script assigns temperature to each grid block of the geomodel using geothermal gradient of 18℃/km.

```
BEGIN{
        RS="\n"
        dip = 0.26          # radians
        T0 = 135            # Temp in degrees C for z = z0
        z0 = 0              # datum for T
        dTdz = -0.018       # C/m, gets colder as z increases upward

        nElemRead = 0
        rX = - sin(dip)
        rZ = cos(dip)

        doCsv = 0           # Toggle csv diagnostics at end of file
                            # 1=on, 0=off; off for TOUGH .dat creation}
{if (match($0,"ELEME")){
        print$0
#       Get current elements
        getline
        while(!match($0,"^ *$") && NF>1) {
                nElemRead++
                print $0
                eName = substr($0,1,5)
                eNameV[nElemRead]=eName
                x[eName] = substr($0,51,10)
                y[eName] = substr($0,61,10)
                z[eName] = substr($0,71,10)
                getline         }
        print $0        }

# Sort through the INCON records
else if (match($0,"INCON")) {
        print $0
        getline
        for (i=1;i<= nElemRead;i++) {
                print $0
                eName = substr($0,1,5)
                getline
                zT[eName] = rZ * z[eName] + rX * x[eName]
                p = substr($0,1,20)
                T[eName] = T0 + dTdz * (zT[eName] - z0)
                printf(" %19g %19g\n", p, T[eName])
                getline         }
        print $0        }
```

```
else {   print $0          }}
END {
if  (doCsv) {
printf("ELEM,  x,  y,  z.in,  z.out,  T.out\n")
for  (i=1;i<=nElemRead;i++) {
printf("%5s,  %10g,  %10g,  %10g,  %10g,  %10g\n",  eNameV[i],x[eNameV[i]],
y[eNameV[i]],  z[eNameV[i]],  zT[eNameV[i]],  T[eNameV[i]])          }}}
```

E.2 R Code for Quiescent Period Calculation in Geothermal Systems

R code loads an output file for Case 2 and calculates differences in aqueous phase flow values for each grid block after 10, 100, 1000, 10000, and 100000 years since initialization.

```
> case2flo <- read.csv("case2flo.csv")
> summary(case2flo)
      TIME                FLOAQ                  t
 Min.   :3.15e+08   Min.   :-1.490e-02   Min.   :    10
 1st Qu.:3.15e+09   1st Qu.:-2.522e-07   1st Qu.:   100
 Median :3.15e+10   Median : 0.000e+00   Median :  1000
 Mean   :7.00e+11   Mean   : 6.884e-07   Mean   : 22222
 3rd Qu.:3.15e+11   3rd Qu.: 3.600e-07   3rd Qu.: 10000
 Max.   :3.15e+12   Max.   : 2.910e-02   Max.   :100000
> flon <- by(case2flo,case2flo$t,data.frame)
> flon12<-flon[[1]]$FLOAQ-flon[[2]]$FLOAQ
> summary(flon12)
      Min.    1st Qu.     Median       Mean    3rd Qu.       Max.
-1.436e-02 -2.062e-07  0.000e+00  2.889e-06  5.152e-06  2.839e-02
> summary(flon[[1]])
      TIME                FLOAQ                  t
 Min.   :3.15e+08   Min.   :-1.490e-02   Min.   :10
 1st Qu.:3.15e+08   1st Qu.:-1.110e-06   1st Qu.:10
 Median :3.15e+08   Median : 0.000e+00   Median :10
 Mean   :3.15e+08   Mean   : 3.166e-06   Mean   :10
 3rd Qu.:3.15e+08   3rd Qu.: 8.157e-06   3rd Qu.:10
 Max.   :3.15e+08   Max.   : 2.910e-02   Max.   :10
> flon23<-flon[[2]]$FLOAQ-flon[[3]]$FLOAQ
> summary(flon23)
      Min.    1st Qu.     Median       Mean    3rd Qu.       Max.
-6.768e-04 -1.825e-08  0.000e+00  2.760e-07  4.242e-07  1.060e-03
> flon34<-flon[[3]]$FLOAQ-flon[[4]]$FLOAQ
> summary(flon34)
      Min.    1st Qu.     Median       Mean    3rd Qu.       Max.
-4.530e-07  0.000e+00  0.000e+00  4.618e-10  1.000e-09  4.860e-07
> flon45<-flon[[4]]$FLOAQ-flon[[5]]$FLOAQ
> summary(flon45)
   Min. 1st Qu.  Median    Mean 3rd Qu.    Max.
      0       0       0       0       0       0
```

R code loads an output file for Case 8 and calculates differences in aqueous phase flow values for each grid block after 10, 100, 1000, 10000, and 100000 years since initialization.

```
> case8flo <- read.csv("case8flo.csv")
> summary(case8flo)
      TIME               FLOAQ                   t
 Min.   :3.15e+08   Min.   :-2.410e-02   Min.   :     10
 1st Qu.:3.15e+09   1st Qu.:-4.920e-07   1st Qu.:    100
 Median :3.15e+10   Median : 0.000e+00   Median :   1000
 Mean   :7.00e+11   Mean   : 6.777e-07   Mean   :  22222
 3rd Qu.:3.15e+11   3rd Qu.: 6.790e-07   3rd Qu.:  10000
 Max.   :3.15e+12   Max.   : 3.880e-02   Max.   :100000
> flo <- by(case8flo,case8flo$t,data.frame)
> flo12<-flo[[1]]$FLOAQ-flo[[2]]$FLOAQ
> summary(flo12)
      Min.    1st Qu.     Median       Mean    3rd Qu.       Max.
-2.307e-02 -7.455e-07  0.000e+00  2.894e-06  6.100e-06  3.745e-02
> flo23<-flo[[2]]$FLOAQ-flo[[3]]$FLOAQ
> summary(flo23)
      Min.    1st Qu.     Median       Mean    3rd Qu.       Max.
-1.319e-03 -8.325e-08  0.000e+00  2.462e-07  6.529e-07  2.028e-03
> flo34<-flo[[3]]$FLOAQ-flo[[4]]$FLOAQ
> summary(flo34)
      Min.    1st Qu.     Median       Mean    3rd Qu.       Max.
-1.787e-06  0.000e+00  0.000e+00  5.768e-10  1.700e-09  2.077e-06
> flo45<-flo[[4]]$FLOAQ-flo[[5]]$FLOAQ
> summary(flo45)
      Min.    1st Qu.     Median       Mean    3rd Qu.       Max.
-1.000e-08  0.000e+00  0.000e+00  2.173e-12  0.000e+00  1.000e-08
```

E.3 R Code for Wellbore Cooling Cases

R code loads an output file with temperatures from the 3 runs after 30 years of wellbore cooling.

```
> cool <- read.csv("cooling1.csv")
> summary(cool)
       T1              T10              T100             T1T10              T10T100
 Min.   : 50.0   Min.   : 50.0   Min.   : 49.97   Min.   :-8.39230   Min.   :-11.2928
 1st Qu.:136.2   1st Qu.:103.0   1st Qu.: 57.07   1st Qu.:-0.05849   1st Qu.:  0.6618
 Median :140.5   Median :134.7   Median : 72.80   Median : 0.54999   Median : 16.0653
 Mean   :139.3   Mean   :121.1   Mean   : 95.36   Mean   :18.20678   Mean   : 25.7810
 3rd Qu.:146.1   3rd Qu.:139.0   3rd Qu.:136.84   3rd Qu.:35.05016   3rd Qu.: 50.7900
 Max.   :152.3   Max.   :149.2   Max.   :145.06   Max.   :86.64973   Max.   : 81.4759
     T1T100
 Min.   :-12.9246
 1st Qu.:  0.7111
 Median : 45.2454
 Mean   : 43.9878
 3rd Qu.: 88.2637
 Max.   : 99.8965
```

E.4 R Code for Selecting Model and Plotting with Contour Plot

R code runs stepwise regression to select the model with the most significant factors and presents the result as a contour plot of thickness and dip versus energy output.

```
# define initial model for energy output
fit.energy <- lm(energy ~ perm * h * dip * Ra * convec * co2,data=ener)

# use the package for stepwise regression
require(MASS)

# find model using Akaike An Information Criterion
step.energy <- stepAIC(fit.energy, direction="both")

# define new model based on what stepAIC has found
fit.energy.final <- lm(energy ~ dip + convec+dip:convec + h,data=ener)

# make grid with h and dip
g.h.dip <- expand.grid(h=h,dip=dip)
g.h.dip <- data.frame(g.h.dip,convec=rep(0,25))

# predict value of energy output based on the model
g.h.dip <- data.frame(g.h.dip,ener.model=predict(fit.energy.final,g.h.dip))

# contour plot the result
filled.contour(h, dip, plot.var, color=terrain.colors,xlab="Thickness,
m",ylab="Dip, degrees", main="Energy output (J)")
```

Vita

Tatyana Plaksina attended Lawrence University, Appleton, Wisconsin, and graduated in 2005. She earned a Bachelor of Arts in mathematics and computer science with minor in art history. She joined the Department of Petroleum Engineering at Louisiana State University and is currently a candidate for a Master of Science in Petroleum Engineering degree to be awarded in August 2011.